

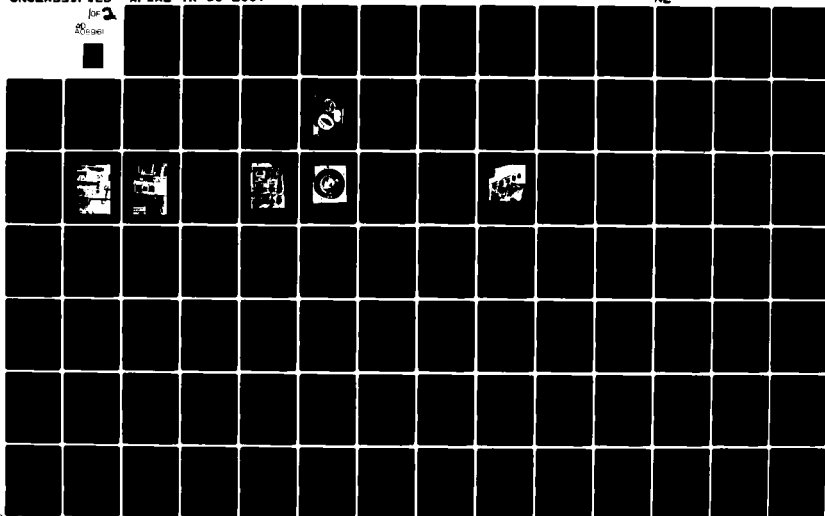
AD-A089 161

AIR FORCE WRIGHT AERONAUTICAL LABS WRIGHT-PATTERSON AFB OH F/G 21/5
AN EVALUATION OF THE USEFULNESS OF TWO MATH MODELS FOR PREDICTI--ETC(U)
APR 80 D R SCHULZE
AFWAL-TR-80-2007

UNCLASSIFIED

NL

for
AD-A089 161



AD A089161

AFWAL-TR-80-2007

AN EVALUATION OF THE USEFULNESS OF TWO MATH MODELS
FOR PREDICTING PERFORMANCE OF A 100 MM BORE,
ANGULAR CONTACT, HIGH SPEED, THRUST BEARING

Dale R. Schulze
Lubrication Branch
Fuels and Lubrication Division

April 1980

TECHNICAL REPORT AFWAL-TR-80-2007

Final Report for Period May 1977 - December 1978

DTIC
SELECTED
SEP 1 1980

Approved for public release; distribution unlimited.

DDC FILE COPY

AERO PROPULSION LABORATORY
AIR FORCE WRIGHT AERONAUTICAL LABORATORIES
AIR FORCE SYSTEMS COMMAND
WRIGHT-PATTERSON AIR FORCE BASE, OHIO 45433

80 9 100

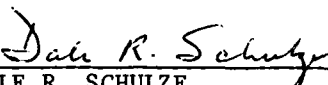
1

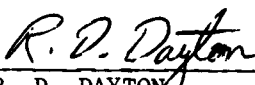
NOTICE

When Government drawings, specifications, or other data are used for any purpose other than in connection with a definitely related Government procurement operation, the United States Government thereby incurs no responsibility nor any obligation whatsoever; and the fact that the government may have formulated, furnished, or in any way supplied the said drawings, specifications, or other data, is not to be regarded by implication or otherwise as in any manner licensing the holder or any other person or corporation, or conveying any rights or permission to manufacture use, or sell any patented invention that may in any way be related thereto.

This report has been reviewed by the Office of Public Affairs (ASD/PA) and is releasable to the National Technical Information Service (NTIS). At NTIS, it will be available to the general public, including foreign nations.

This technical report has been reviewed and is approved for publication.


DALE R. SCHULZE
Project Engineer


R. D. DAYTON
Acting Chief, Lubrication Branch

FOR THE COMMANDER


ROBERT D. SHEKRILL
Chief, Fuels and Lubrication Division

"If your address has changed, if you wish to be removed from our mailing list, or if the addressee is no longer employed by your organization please notify AFWAL/POSL, W-PAFB, OH 45433 to help us maintain a current mailing list".

Copies of this report should not be returned unless return is required by security considerations, contractual obligations, or notice on a specific document.

SECURITY CLASSIFICATION OF THIS PAGE (When Data Entered)

REPORT DOCUMENTATION PAGE		READ INSTRUCTIONS BEFORE COMPLETING FORM
1. REPORT NUMBER 14 AFWAL-TR-80-2007	2. GOVT ACCESSION NO. AD-A089 1649	3. RECIPIENT'S CATALOG NUMBER
4. TITLE (and Subtitle) AN EVALUATION OF THE USEFULNESS OF TWO MODELS FOR PREDICTING PERFORMANCE OF A 100 mm BORE, ANGULAR CONTACT, HIGH SPEED, THRUST BEARING.		5. TYPE OF REPORT & PERIOD COVERED Final Technical Report, May 1977 - December 1978
7. AUTHOR(s) Dale R. Schulze		6. PERFORMING ORG. REPORT NUMBER
9. PERFORMING ORGANIZATION NAME AND ADDRESS Aero Propulsion Laboratory (POSL) Air Force Wright Aeronautical Laboratories (AFSC) Wright-Patterson Air Force Base, Ohio 45433		8. CONTRACT OR GRANT NUMBER(s)
11. CONTROLLING OFFICE NAME AND ADDRESS Aero Propulsion Laboratory (POS) Air Force Wright Aeronautical Laboratories (AFSC) Wright-Patterson Air Force Base, Ohio 45433		10. PROGRAM ELEMENT, PROJECT, TASK AREA & WORK UNIT NUMBERS Project 3048 Task 304806 Work Unit 30480619
14. MONITORING AGENCY NAME & ADDRESS (if different from Controlling Office)		12. REPORT DATE April 1980
		13. NUMBER OF PAGES 96
		15. SECURITY CLASS. (of this report) UNCLASSIFIED
		15a. DECLASSIFICATION/DOWNGRADING SCHEDULE
16. DISTRIBUTION STATEMENT (of this Report) Approved for Public Release; Distribution Unlimited.		
17. DISTRIBUTION STATEMENT (of the abstract entered in Block 20, if different from Report)		
18. SUPPLEMENTARY NOTES		
19. KEY WORDS (Continue on reverse side if necessary and identify by block number) Bearings, Lubrication Systems, Computer Models, Cage Dynamics, Bearing Performance.		
20. ABSTRACT (Continue on reverse side if necessary and identify by block number) New designs for mainshaft thrust bearings for gas turbine engines are derived from mathematical and experimental analyses. The predictions of two bearing computer models, DREB and SHABERTH, being used by the Aero Propulsion Laboratory, were compared to experimental data generated by this study. This test bearing was a 100 mm bore, angular contact, ball bearing which was designed for R&D. <i>over</i>		

(Continued)

1

~~SECURITY CLASSIFICATION OF THIS PAGE(When Data Entered)~~

✓ Overall, the SHABERTH model was found to be a more practical tool for preliminary bearing design. However, DREB showed promise of being a valuable tool for diagnosing the dynamics of the bearing cage. This study also presents a new method for measuring three-dimensional kinematics of the bearing cage.

A bibliography of the pertinent literature is included.

SECURITY CLASSIFICATION OF THIS PAGE(When Data Entered)

FOREWORD

This report describes an in-house effort conducted by personnel of the Lubrication Branch (POSL), Fuels and Lubrication Division (POS), Aero Propulsion Laboratory, Air Force Wright Aeronautical Laboratories, Wright-Patterson Air Force Base, Ohio, under Project 3048, "Fuels and Lubrication Technology," Task 304806, "Lubrication," Work Unit 30480619, "Bearing Dynamics Research for Propulsion Systems."

The work reported herein was performed during the period May 1977 to December 1978 under the direction of Dr. James Dill (AFWAL/POSL), project engineer. The author submitted the report in January 1980.

The author wishes to thank the following APL personnel who assisted in the performance of this effort: Ron Dayton (project engineer), Steve Jackson, Bill Smiley and Bob Esch (technicians).

A

TABLE OF CONTENTS

SECTION	PAGE
I INTRODUCTION	1
1. Background and Objectives	1
2. Brief Summary of Results	6
II COMPUTER PROGRAMMING	9
1. Input	9
2. Execution and Output	9
III EXPERIMENTATION	17
1. Test Rig, Instrumentation and Calibration	17
2. Experimental Procedures	33
a. Parametric Study	33
b. Dynamic Study	36
1) Lissajous Tests	36
2) Frequency Spectrum Tests	38
IV RESULTS	39
1. Comparison of Analytical Data which were not Measured in the Experimental Phase	39
a. Stresses and Angle of Ball-Race Contact	39
b. EHD Film Thickness at Ball-Race Contacts	39
c. Fatigue Life	46
2. Comparison of Analytical Data to the Experimental Parametric Results	48
a. Bearing Torque	48
b. Heat Generation	48
c. Cage Orbital Speed and Skidding	53

TABLE OF CONTENTS (Cont'd)

SECTION	PAGE
3. Comparison of DREB Output to Experimental Dynamic Study Results	53
a. <i>Lissajous Figure Test Results</i>	53
b. Frequency Spectrum Analysis Test Results	61
V CONCLUSIONS AND RECOMMENDATIONS	66
APPENDIX	69
REFERENCES	85
BIBLIOGRAPHY	86

LIST OF ILLUSTRATIONS

FIGURE	PAGE
1 Computer Programs Flowchart, DREB & SHABERTH	5
2 Test Bearing, 100 mm Bore Diameter	8
3 30,000 rpm Bearing Test Rig	18
4 Test Rig Console	19
5 Drawing of Test Rig Cross-Section	20
6 Lubricant Flow and Temperature Controls	21
7 Partially Disassembled Test Housing	22
8 Proximitors and Power Supply	25
9 Probe System Operation	27
10 Probe Signal "De-biasing" Circuit	28
11 Initial Clearances of Probes	29
12 Axial View, Probe Locations	31
13 Radial View, Probe Locations	32
14 Proximity Probes Calibration Curves	34
15 Ball-Inner Race Contact Stress	40
16 Ball-Outer Race Contact Stress	41
17 Ball-Inner Race Contact Angle	42
18 Ball-Outer Race Contact Angle	43
19 Ball-Inner Race Contact Film Thickness	44
20 Ball-Outer Race Contact Film Thickness	45
21 L-10 Fatigue Life	47
22 Bearing Torsion, Experimentally - Obtained Sweep for 4448 N Thrust Case	49
23 Experimental and Predicted Torsion	50
24 DREB Plot of Torque Variation with Time	51

LIST OF ILLUSTRATIONS (Concluded)

FIGURE	PAGE
25 Heat Generation	52
26 DREB Power Loss	54
27 Cage Orbital Speed	55
28 DREBP Cage Orbit Speed Variation with Time	56
29 Cage Whirl Images Photographed on Oscilloscope	57
30 Inner Ring - Cage	59
31 DREBP of Cage Mass Center Position	60
32 DREBP of Cage Mass Center Velocity	62
33 Cage Radial Motion	64
34 Cage Axial Motion	65

AFWAL-TR-80-2007

LIST OF TABLES

TABLE	PAGE
1 Test Lubricant (MIL-L-7808G) Characteristics	7
2 Test Bearing Description	7
3 Computer Programs Input Data	10-15

SECTION I
INTRODUCTION

1. BACKGROUND AND OBJECTIVES

Main shaft, angular contact, ball bearings on current aircraft gas turbine engines support thrust loads of thousands of pounds at speeds in the range of 2.0 million DN (DN is defined as the bearing bore diameter in millimeters times the shaft speed in revolutions per minute). The quest for higher thrust to weight ratios in future power plants will demand still higher shaft speeds and larger shaft diameters. This calls for the design of bearings operable to higher DN values.

Several different types of bearings have been tested in order to achieve this higher performance. Ceramic rolling element bearings, gas bearings, and tapered roller bearings all have been tested for thrust bearings applications with varying degrees of success. But the conventionally used, angular contact ball bearing has proved to be currently the most reliable type of bearing for use in large turbine engines.

Traditionally the main objective in designing such bearings has been to reduce the incidence of spalling fatigue failure of the races for a large number (10^9) of stress cycles. The Hertzian stresses typically generated in the ball-race contacts exceed 200 ksi. Therefore, the conventional analyses deal primarily with maximizing the load carrying capability of the bearing by judicious selection of materials and careful design of the internal bearing geometry. Most turbine engine bearings today are made from M-50 steel.

Just as critical to bearing performance as the material and geometry is the type of lubricant used, the method of supplying the lubricant to the bearing, and the amount supplied. The lubricant most widely used in Air Force turbine engines, a synthetic ester meeting specification MIL-L-7808G, was also used in this study and is described in Table 1. The lubricant acts both as a separator between interfacing bearing components and as a bearing coolant. Both races should be completely

wetted with a contaminant-free lubricant film to prevent dry-metallic contact. This is normally accomplished by using circumferentially spaced lubricant jets pointed at the bearing internal clearances or by centrifugally supplying lubricant via a hollow shaft and inner ring channels. Copious amounts of lubricant should be supplied to the bearing in order to prevent excessive heat generation which may increase the race wear rate by thinning the separating film in the ball-race contacts. This heat generation is a result of the drag of the balls as they translate through the lubricant film, the churning moment that results from their own rotation, and the energy lost during the elastohydrodynamic (EHD) lubrication at the ball-race contacts.

EHD lubrication essentially is the combination of hydrodynamic lubrication and the elastic deformation of the contacting rolling bodies. This deformation occurs in proportion to the applied load but is also slightly affected by the thickness and the viscosity of the fluid film between the surfaces. The extent of EHD lubrication (which is discussed extensively in the literature - See Bibliography) affects ball traction, the contact force generated which resists relative motion of the bearing surfaces. Traction determines whether the ball rolls or skids on the race since it is the moment caused by this force which causes the rotation of the ball. EHD lubrication is "fully established" when a completely formed film of lubricant exists between the rolling surfaces.

The aforementioned design criteria are essentially considerations for minimizing race wear. But by using improved materials, contaminant-free and effective lubrication and proper design of the balls and races, the frequency of wear failures has been decreased.

Of growing concern to bearing designers are the motions of the ball separator during high speed operation. This separator, commonly called the cage, is a cylindrical ring of tough metal (such as AISI 4340) with pockets to contain the balls. The only purpose of the cage is to keep the balls evenly spaced and in relatively smooth orbits about the bearing center. A small clearance (0.015 - 0.030 inch) between the cage and the

riding surface on each side of the race of one of the rings (for this study the inner ring) guides the rotation of the cage. At some high speed, a supporting hydrodynamic film develops in this clearance, much like in a journal bearing.

Kannel (References 1 and 2) described the cage dynamics as a "hidden cause" of bearing failure. The orbiting balls push and pull on the cage and induce a spectrum of cage oscillations. This actually is accompanied by the hydrodynamic forces between the cage and the guiding ring to result in a "whirling" of the cage mass center about the bearing center. At certain critical speeds and especially during adverse conditions such as an oil interruption or an unbalanced shaft, this whirling may grow in amplitude to the point of cage-ring contact, resulting in tremendous heat generation and/or fracture fatigue of the cage. Clearly it is necessary to design the cage with the strength to withstand such forces, and yet be small enough in mass to allow nearly free orbiting of the balls. Also it is critical to maintain the proper clearances between the cage and rings by allowing for thermal and centrifugal growth.

From the discussion so far, it is apparent that new and reliable bearing methods encompassing the conventional analyses and consideration of the cage motions should be developed.

In recent years, the design of high-speed rolling element bearings has been greatly expedited by the use of computer program simulations. These models have performed the complex task of combining the huge number of design variables with the desired test conditions to obtain calculations for the endurance life and power consumption and many other bearing performance parameters. Some recent models have even attempted to simulate the six-degree-of-freedom motions of the balls and cage. Even though these models are widely used for bearing design and diagnostics, few of them have actually been proven by comparing their output to data from actual bearing operation.

Coe and Zaretsky (Reference 3) compared two analytical models to laboratory tests using a 120 mm bore, angular contact bearing. Unfortunately, neither of their models could predict the movements of the cage and balls for all their degrees of freedom. In addition, their bearing test rig had no instrumentation for measuring these movements.

Walters (Reference 4) and Gupta (Reference 5) have developed formulations for predicting the three-dimensional cage motions, but their analyses have not been verified experimentally. Kannel (Reference 2) studied cage motions in the radial plane of low speed, antenna bearings but did not measure the motions in the shaft axial direction.

In this study, cage motion was measured for the three axes of a 100 mm bore, angular contact, ball bearing to produce part of an experimental data base for comparison with the analytical predictions from two bearing mathematical models. This information along with other experimental data obtained on a high-speed bearing test rig was analyzed to determine the relative usefulness of the models as bearing design tools. It was not the purpose of this study to provide a detailed comparison of the theoretical bases of each model. That information is most fairly presented in the literature.

The two computer programs compared in this study were written by two leaders in bearing industrial research. One program was developed by SKF Industries, Inc. and was titled "SHABERTH, A Shaft-Bearing Thermal Analysis" (References 6 and 7). The other program was written by Mechanical Technology, Inc. (MTI) and was called "DREB, The Dynamics of Rolling Element Bearings" (References 8, 9, 10 and 11). Figure 1 shows a flow chart comparison of the two programs.

These models had widely different main objectives. SHABERTH was the more conventional, quasi-dynamic analysis in which the balls and cage were restricted to a single path on the races. The inertial forces of the ball and cage were obtained using approximate values for the respective accelerations and other simplifying assumptions. The primary features of

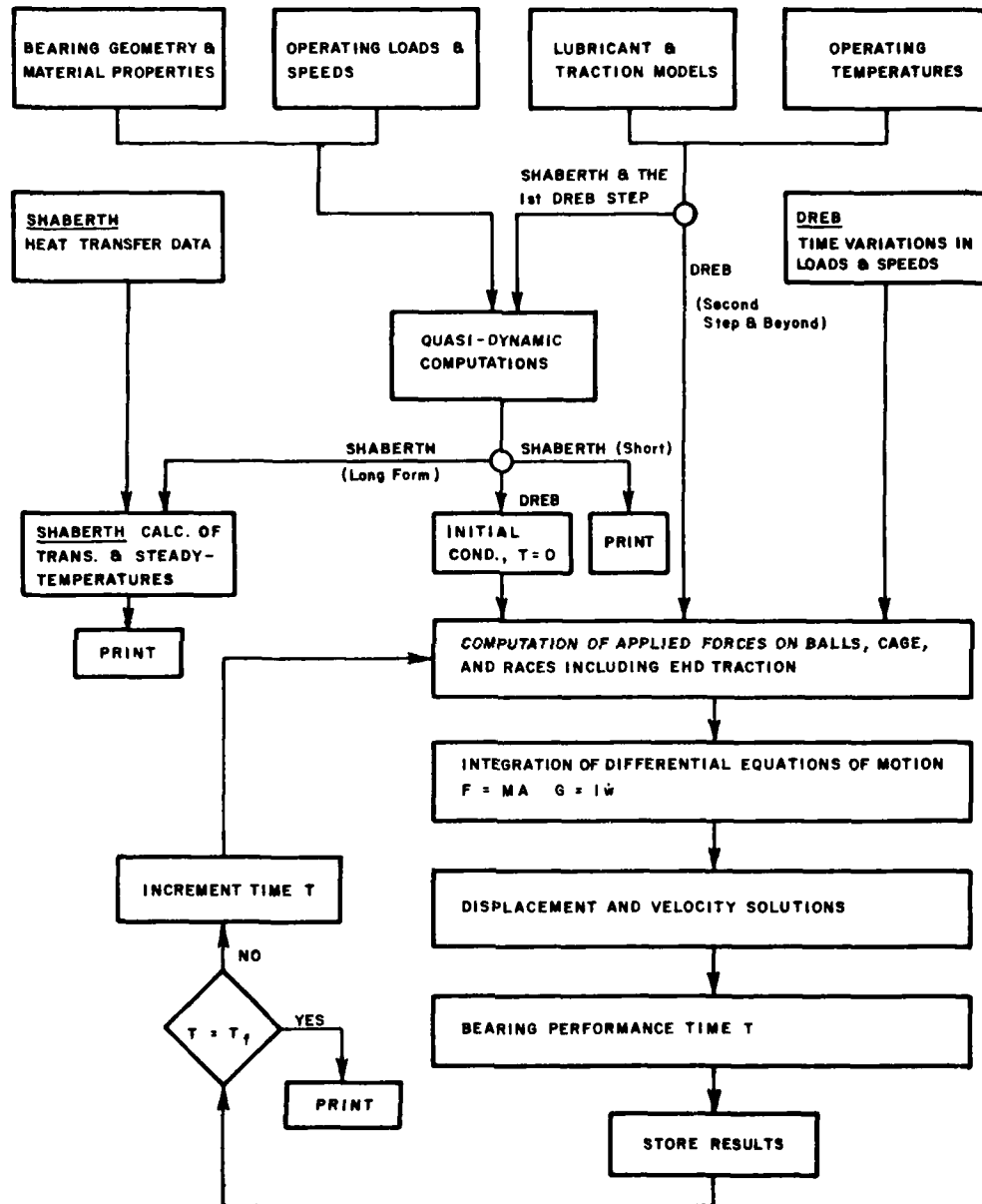


Figure 1. Computer Programs Flowchart DREB and SHABERTH

SHABERTH was its ability to predict operating temperatures at various locations in the shaft/bearing system. This could be done by using the calculated heat generation rates within the bearing together with the heat transfer characteristics of the system.

On the other hand, DREB was a dynamic analyses in which the laws of motion were not approximated and the balls and cage were not restricted to only one orbiting path on the races. However, DREB did not have the capability to calculate temperatures in the shaft/bearing system.

Despite the varying objectives of the models, many of their numerical results describing bearing performance could be compared together. It was known before this study, however, that because DREB contained formulations necessary for the dynamic analyses, it required much more computer time to execute than did SHABERTH. DREB also provided much more total output than SHABERTH. Therefore, a secondary objective of this study was to use SHABERTH in its most simplified form and to determine if its data was sufficiently accurate to take advantage of its economy. The simplified form involved the omission of the thermal routine for calculating temperature maps.

The bearing used in this study was designed solely for research and development purposes with the objective of long-lived operation to 3.0 million DN. Incorporated into its design were many of the best characteristics of thrust bearings currently used on the high-speed, mainshafts of large gas turbine engines. This test bearing is described in Table 2 and is illustrated in Figure 2.

2. BRIEF SUMMARY OF RESULTS

In the overall evaluation of the performance of the two programs, it was learned that SHABERTH was the preferred program for preliminary bearing design studies based on its lower cost of operation. The DREB dynamic model, however, was proven to be a very significant achievement in the progression of analytical techniques for studying bearing behavior. The results obtained in this study provided a substantial basis for confidence in DREB as a diagnostic tool.

TABLE 1

TEST LUBRICANT (MIL-L-7808G) CHARACTERISTICS

- Kinematic Viscosity:	
at 100°F	11.0 Centistokes
at 210°F	3.0 Centistokes
- Flash Point:	400°F
- Evaporation Loss after 6.5 Hours:	
at Sea Level, 400°F	25% max
at 40,000 ft, 400°F	50% max
- Pitting Fatigue:	100 hrs
- Change from Original Viscosity at 100°F: (after 72 Hours at 347°F)	-5 to +15%
- Change from Original Total Acid Number:	0.3 max

TABLE 2

TEST BEARING DESCRIPTION

- angular contact, ball, split inner ring
- 18 balls
- 100 mm bore diameter
- designed for 30,000 rpm by WPAFB, AFAPL
- manufactured by Marlin Rockwell, Division of TRW
- inner race guided cage
- material of balls and rings: M-50 steel (Rockwell 62C)
- cage material: AISI 4340 steel (Rockwell 28-32C) with silver plating (.001 - .002 in.)
- IRC (Internal Radial Clearance)
- through-inner-race lubrication slots

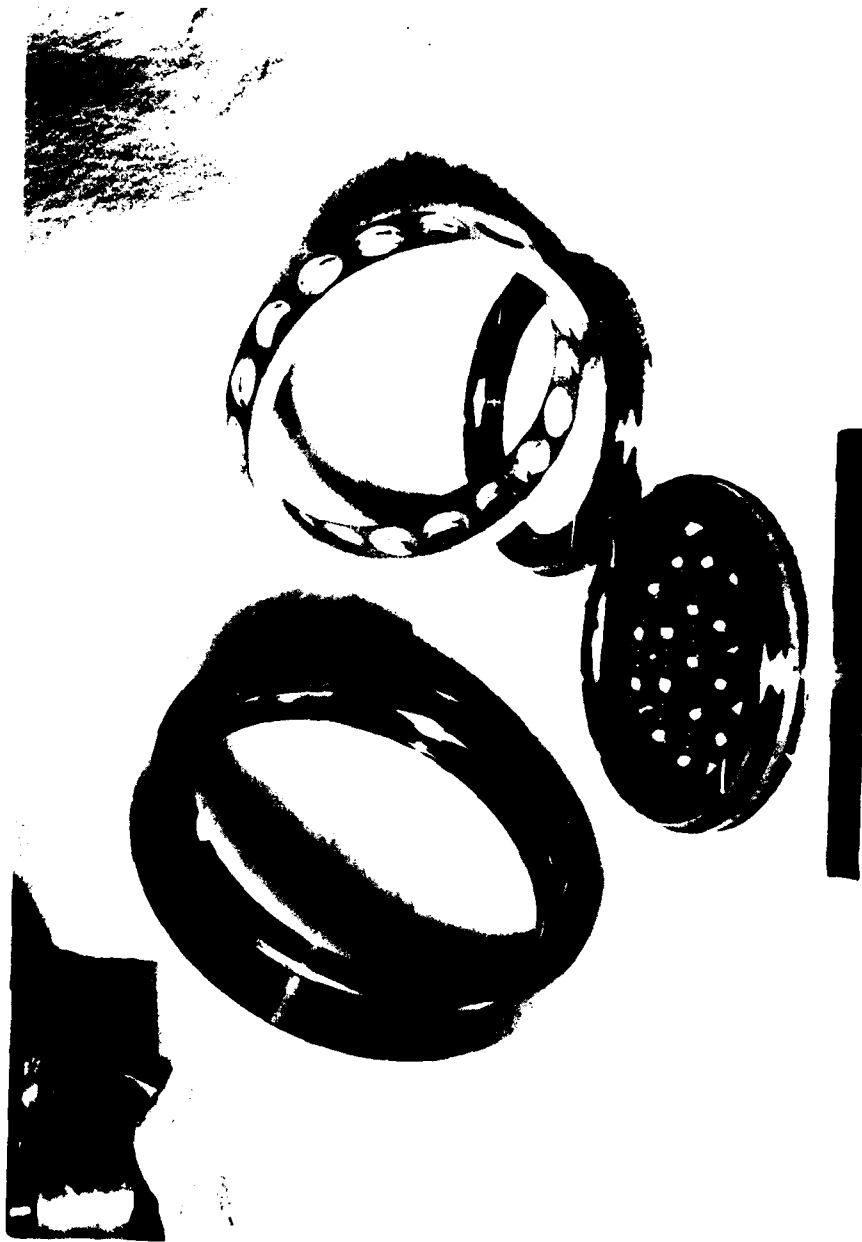


Figure 2. Test Bearing, 100 mm Bore (Shown with six inch ruler)

SECTION II

COMPUTER PROGRAMMING

1. INPUT

DREB and SHABERTH were programmed for use on the CDC 6600 digital computer at WPAFB by taping the card source deck into permanent and local files which could be called for execution of the particular bearing case. For this study, the programs were inputted with data describing the 100 mm test bearing and actual experimental conditions. The amount of input data required for DREB was essentially the same as for SHABERTH although DREB required about 40 IBM cards as compared to 25 for SHABERTH.

Table 3 is a list of the input data required for the programs. Those parameters marked "D" were values which were inputted by default.

2. EXECUTION AND OUTPUT

Both DREB and SHABERTH required several preliminary runs of the computer before the errors in the input data were corrected. There was a significant problem concerning interpretation of the output, especially for DREB. By careful study of the user's manuals and correspondence with the authors of the programs, most of the questions were answered. Part of the problem with DREB was due to the immense quantity of output data due to the dynamic simulation, while the accompanying documentation provided for the user was less than fully descriptive.

SHABERTH required about 20 seconds of computation time and printed about 150 lines of output for each load/speed condition. DREB ran much longer, depending on the number and frequency of dynamic computations requested and the user specified truncation error for the numerical integrations. The DREB modelled bearing usually reached a "steady-state" condition after roughly 1,000 seconds of computation time. "Steady-state" was defined as the point at which the cage began its periodic motions about some average position. In some cases, this periodicity did not occur until after about 1,500 seconds of computation time. Unfortunately,

TABLE 3
COMPUTER PROGRAMS INPUT DATA

PARAMETER	UNITS	VALUE	DREB	SHABERTH
GEOMETRY				
Inner Race Half Width	mm	25.000		x
Shaft Inner Diameter	mm	20.000	x	x
Bearing Bore Diameter	mm	100.000	x	x
Inner Ring Outer Diam.	mm	127.000	x	x
Outer Ring Inner Diam.	mm	155.000	x	x
Bearing Outer Diameter	mm	180.000	x	x
Housing Outer Diameter	mm	205.000		x
Pitch Diameter	mm	140.000	x	x
Diametral Clearance, O.R.	mm	2.020	x	D
Contact Angle	Deg	25	x	x
Cage Pocket Clearance	mm	.826	x	x
Rail-Land Width	mm	4.000	x	x
Rail-Land Diameter	mm	128.470	x	x
Rail-Land Clearance	mm	1.270	x	x
Ball Diameter	mm	19.050	x	x
Outer Race Curvature	--	.520	x	x
Inner Race Curvature	--	.540	x	x
Shaft Width	mm	22.000		x
Inner Ring Width	mm	17.000		x
Outer Ring Width	mm	34.000		x
Housing Width	mm	67.000		x
Cage Inner Diameter	mm	129.000	x	
Cage Outer Diameter	mm	148.800	x	

TABLE 3 (Continued)

PARAMETER	UNITS	VALUE	DREB	SHABERTH
GEOMETRY (Cont'd)				
Cage Width	mm	27.300	x	
Land Edge to Cage Center	mm	13.600	x	
Shaft Outer Diameter	mm	100.000	x	x
MOUNTING DATA				
Radial Mounting Error	mm	0	x	x
Angular Mounting Error	Rad	0	x	x
Radial Spring of Housing	mm/N	Rigid		D
Angular Spring of Housing	Rad/N	Rigid		D
Cold Fit with Shaft	mm	.0050	zero fit	x
Cold Fit with Housing	mm	-.0380	zero fit	x
MATERIAL PROPERTIES OF RINGS, BALLS, SHAFT, AND HOUSING				
Modulus of Elasticity	N/mm ²	204083.0	x	D
Poissons Ratio	--	.30	x	D
Weight Density	Kg/m ³	7.806	x	D
Coef. of Thermal Expansion	1/C	1.224×10^{-5}		D
Inner Ring Material	--	SPEC		x
Outer Ring Material	--	SPEC		x
Inner Ring Life Factor	--	5.0		x
Outer Ring Life Factor	--	5.0		x
Inner Race CLA Roughness	microns	.08		x
Outer Race CLA Roughness	microns	.08		x
Ball CLA Roughness	microns	.04		x

TABLE 3 (Continued)

PARAMETER	UNITS	VALUE	DREB	SHABERTH
MATERIAL PROPERTIES OF RINGS, BALLS, SHAFT, AND HOUSING (Cont'd)				
Outer Race RMS Asperity Slope	--	2.0		x
Inner Race RMS Asperity Slope	--	2.0		x
Ball RMS Asperity Slope	--	2.0		x
Asperity Friction Coef.	--	.10		x
LOAD/SPEED DATA				
Radial Force	N	0	x	x
Axial Force	N	SPEC	x	x
Concentric Moment about Z axis	N-mm	0		x
Load Distribution	N-mm	CONCEN.		x
Thrust Line of Action, Y axis	mm	0		x
Inner Ring Speed	RPM	SPEC	x	x
Outer Ring Speed	RPM	0	x	x
External Forces	N	0	x	x
THERMAL DATA (INITIAL)				
Shaft Temperature	deg C	140.0		x
Inner Ring Temperature	deg C	145.0		x
Inner Race Temperature	deg C	150.0	x	x
Ball Temperature	deg C	170.0		x
Outer Race Temperature	deg C	165.0	x	x

TABLE 3 (Continued)

PARAMETER	UNITS	VALUE	DREB	SHABERTH
THERMAL DATA (INITIAL) (Cont'd)				
Outer Ring Temperature	deg C	160.0		x
Housing Temperature	deg C	150.0		x
Bulk Lubricant Temp.	deg C	140.0		x
Inlet Oil Temperature	deg K	405.0	x	
CAGE DATA				
Cage Material	--	SPEC	x	x
Cage Weight	Kgm	.300		x
Cage Type	--	Inner	x	x
TRACTION DATA				
Traction Coef. at Zero Slip	sec/M	0	x	
Traction Coef. at Max Trac	sec/M	.15	x	
Traction Coef. at Infin. Slip	sec/M	.007	x	
Slip at Maximum Traction	M/sec	2.54	x	
Minimum Film Thickness	mm	1.27×10^{-4}	x	
Starvation Parameter	--	5.	x	
Effec. Churning Viscos.	Nsec/M ²	3.46×10^{-4}	x	
Effec. Churning Density	Kgm/m ³	83.07	x	
LUBRICANT DATA				
Lubricant	--	MIL-L-7808G	x	x
Kinematic Viscos, 38°C	M ² /sec	12.76		D
Kinematic Viscos, 99°C	M ² /sec	3.20		D

TABLE 3 (Continued)

PARAMETER	UNITS	VALUE	DREB	SHABERTH
LUBRICANT DATA (Cont'd)				
Density, 15.6°C	Kgm/m ³	.9526		D
Thermal Expansion Coef.	1/C	7.09×10^{-4}		D
Thermal Conductivity	Watts/m ² /C	.152		D
% Lubricant in Cavity	--	100.		x
Film Replen. Thickness	--	.001		x
Ball/Cage Max. Film	m	.000826	x	
PROGRAM CONTROLS				
Print Flag--Debug	--	0		x
Main Loop Iteration	--	0		x
Fit Loop Accuracy	--	.0001		D
Main Loop Accuracy	--	.001		D
EHD/Coulomb Accuracy	--	.0001		D
Function Switch	--	SPEC	x	
Data Monitor Code	--	SPEC	x	
Print Codes	--	SPEC	x	
Integ. Trunc. Error	--	5.0×10^{-4}	x	
Optimization Codes	--	SPEC	x	
Trac. Curve Increm.	--	5.0×10^{-3}	x	
Initial Conditions	--	0	x	
Special Output Indexes	--	SPEC	x	
Selec. of Units Switch	--	SI	x	
Init. Dimensionless Time Step	--	.05	x	

TABLE 3 (Concluded)

PARAMETER	UNITS	VALUE	DREB	SHABERTH
PROGRAM CONTROLS (Cont'd)				
Min. Dimensionless Time Step	--	.005	x	
Max. Dimensionless Time Step	--	1.0	x	
Final Dimensionless Time Step	--	50.0	x	
Fit Iteration	--	5		x
Contact Switches (4)	--	SPEC	x	
Churning Effects Switch	--	2.0	x	
GENERAL				
Bearing Type	--	Ball	x	x
X-Cord. Shaft Section	mm	0		x
No. of Rolling Elements	--	18	x	x
Crav. Accel.	m/sec ²	9.8	x	
Init. Radial Position of Cage Center with Respect to Inner Race	m	1.27×10^{-4}	x	
Init. Rotation of Cage	Deg	0	x	
Race Constraints	--	SPEC	x	

AFWAL-TR-80-2007

the approximately 9,000 lines of output described a total inner race rotation of about one and one-half turns, even though the printed output was requested for only every fifth numerical integration.

Fortunately, DREB also had a plotting routine called DREBP. To use DREBP, the output of the main program for the particular test case was saved in six local data files, any of which could be called depending on what the user wished to see plotted. A smooth curve connecting all the output data was plotted as a function of scaled time which could be converted to real time by multiplication of the appropriate scale factor provided with the plots.

The first step (no integration) printed-out by DREB was the quasi-static solution and contained values similar to those calculated by SHABERTH. The DREB values used for comparison to the SHABERTH values were from the 200th time step so the difference from the DREB dynamic analyses could be studied.

DREB did have a procedure for reducing the amount of computer time needed which involved reducing the number of balls after the general load distribution on all balls was computed once. This assumed that only the loaded balls played a dominant role in determining the overall performance of the bearings. This "effective partial bearing" was not used in this study since the balls theoretically shared equal portions of the thrust load.

SECTION III

EXPERIMENTATION

1. TEST RIG, INSTRUMENTATION AND CALIBRATION

The high-speed bearing test rig (Figure 3) used for the experimentation was designed and built by Southwest Research Institute for the Aero Propulsion Laboratory and was installed at Wright-Patterson AFB during 1970. The machine accommodated the 100 mm bore test bearing and was driven by a 50 HP Eaton Dynamatic, water cooled, variable-speed drive, electric motor. A 9.25-1 step-up gearbox allowed shaft speeds of up to 30,000 rpm, although attaining that speed was rarely attempted because of the vibration of the support equipment that occurred. A magnetic pick-up located over the shaft measured test speed by supplying impulse signals to a digital counter. The test rig instrument console is shown in Figure 4 and a cross-section of the test rig is shown in Figure 5.

Test oil was supplied to the test bearing at a rate of 2 gal/min through three rear jets spaced 120 degrees apart and two front jets. They were directed toward the clearance between the bearing cage and the outer diameter of the bearing inner ring. The oil was scavenged from the test head through two ports located side by side behind the test bearing, into an accumulator located directly below the test head. The oil pump (Figure 6) was equipped with electrical band heaters which could supply 4,660 watts for conversion to heat.

Thrust load was applied to the test bearing by the axial load piston. The reaction thrust load was supported by a ball-thrust retainer. A 45 mm bore, straight roller bearing supported the spline end of the main drive shaft which is shown in Figure 7. Thrust load could be independently applied to the test bearing by a hand-operated pressure regulator on a nitrogen gas bottle.

The thrust load was measured by use of a 350 ohm, temperature compensated, strain gage half-bridge mounted circumferentially on a thin (1/8 inch) section of the main drive shaft between the test

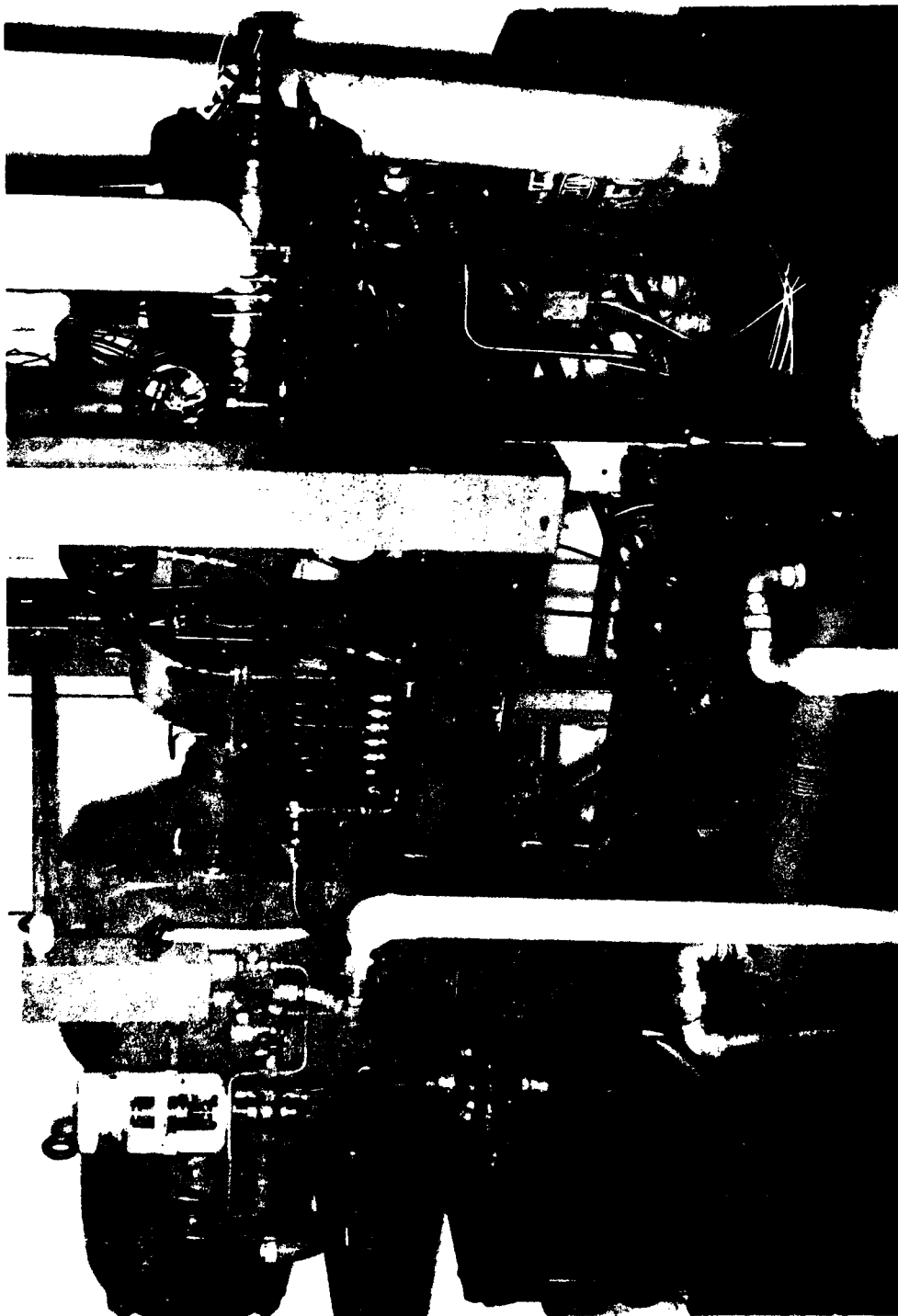


Figure 3. 30,000 rpm Bearing Test Rig

AFWAL-TR-80-2007

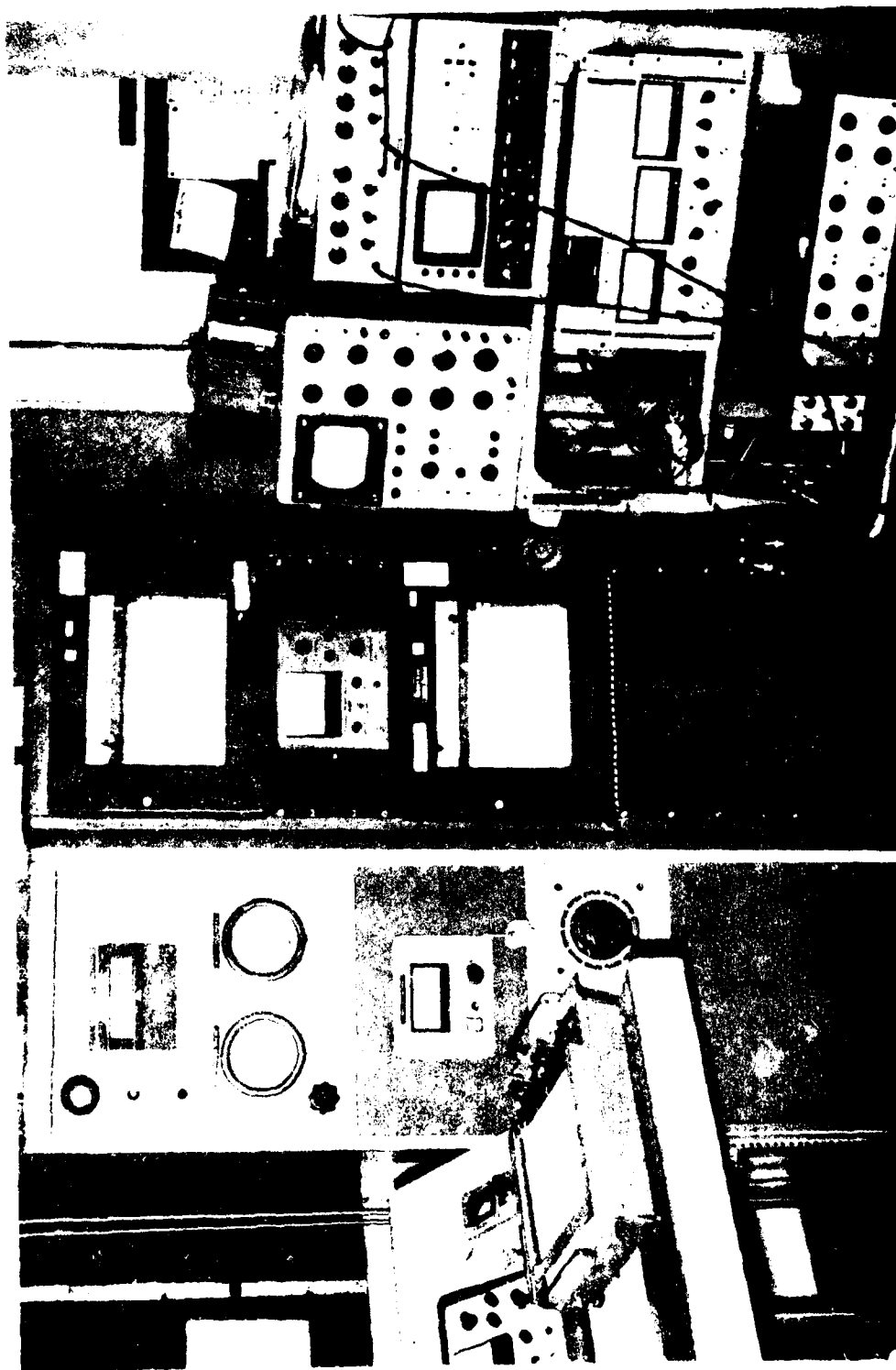


Figure 4. Test Rig Console

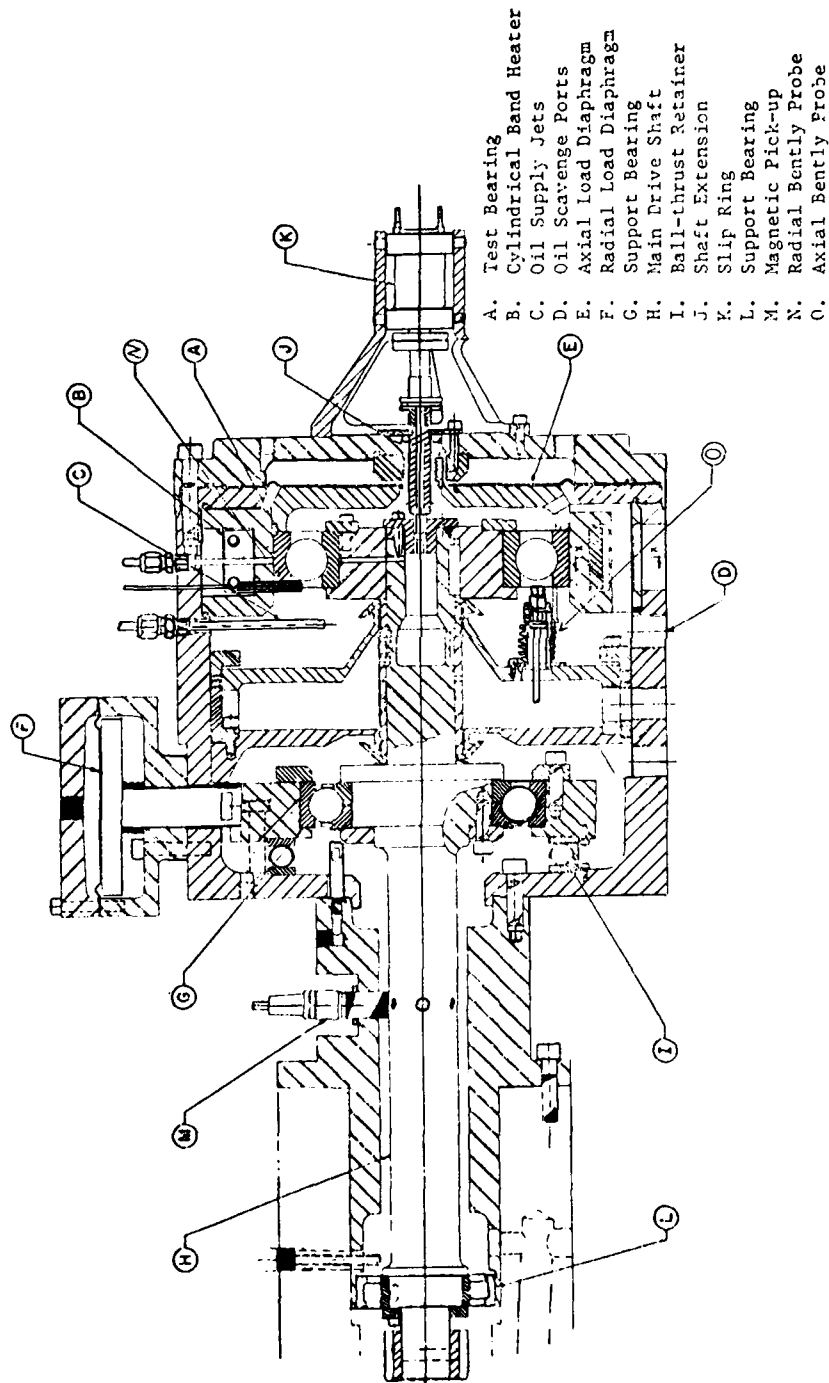


Figure 5. Drawing of Test Rig Cross-Section

ATWAL-100



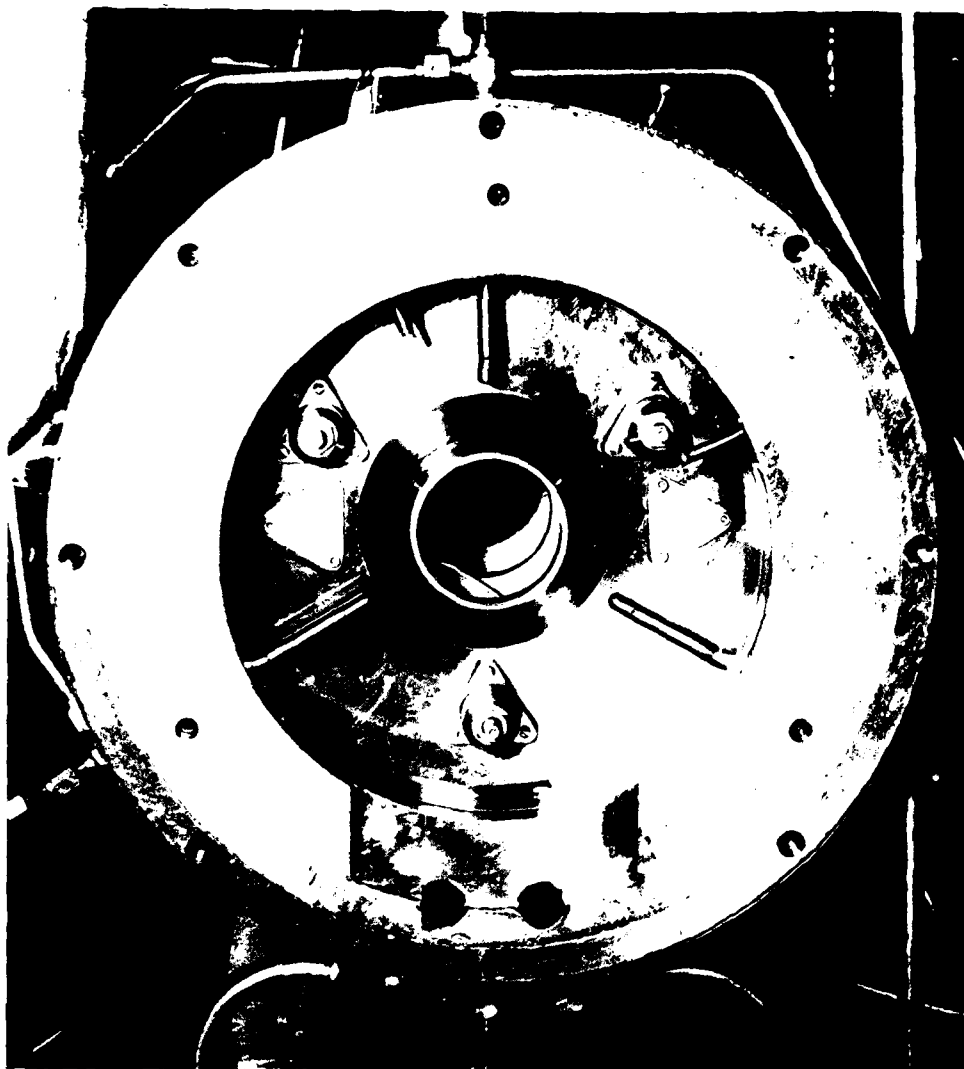


Figure 7. Partially Disassembled Test Housing (Showing Probes and Oil Jets)

bearing and the large support bearings. During operation the thrust strain was measured on an amplifier-indicator. A shaft extension protruded through the sealing bellows in the test chamber end-cover and served as a driver for a freon-cooled, slip ring assembly. The shaft extension was hollow and provided a path for the conductors for torque, thrust and temperature measuring transducers.

Radial load was applied to the test bearing by supplying pressure from the N_2 gas bottle to a radial loading diaphragm which applied a force to the support ball bearing. This force was reacted through the inner race of the test bearing and was measured by multiplication of the loading diaphragm area times the applied gas pressure.

Shaft torque due to test bearing resistance was measured by a temperature and bending compensated, 4-arm, strain-gage bridge also located on the thin section of the shaft. Torsional strain versus shaft speed was transduced, amplified, then recorded on an x-y plotter.

Because the torsional deflection of the shaft due to test bearing torque was normally very small, the increased output from the strain-gage bridge due to temperature changes and thrust loading of the test bearing could not be considered insignificant. Essentially all of the temperature effects in the range of 70-300°F were compensated for by careful installation of the force strain gages such that each leg of the bridge had equal lengths of lead wire. At gage temperatures above 300°F, however, there were "apparent" strain effects until the gage adhesive and coating material (MM GA61) had had sufficient time to post cure at the high temperatures. Therefore, a jet-stream of air was aimed at the strain-gage location on the shaft during use to maintain temperatures below 300°F.

Temperature measurement of the test bearing outer race was accomplished with a thermocouple mounted on the stainless steel sheath. The test bearing inner race temperatures were measured with a sub-miniature size surface type temperature transducer. This low mass, 100 ohm, platinum

sensor was in a machine cavity directly beneath the test bearing inner race. Centrifugal force from shaft rotation pressed the sensor against the inner diameter of the inner race. The sensor leads were circuited to a meter by use of the slip ring assembly. Thermocouples were also located in the oil sump, oil supply jets, and oil drain ports to allow measurement of temperatures at those points. All temperatures were recorded on a multipen, strip chart recorder.

The major modification made to the bearing test rig for the purposes of this study was the installation of five Bently proximity probes to measure the test bearing cage motion. These non-contacting, eddy-current probes were gap to voltage transducers and measured the instantaneous displacement of any conductive material. Figure 7 shows the installed probes with the testing end cover, shaft and test bearing removed. Two probes were mounted 90° apart in the bearing outer housing and were pointed radially inward at the land of the cage outer diameter. Grooves were cut in the bearing outer ring to allow the installation of the probes perpendicular to and directly over the cage land. These two probes measured all radial displacements of the cage. Three other probes were mounted parallel to the shaft and 120° apart on the same diameter on the back seal plate of the bearing housing. They were pointed at the back face of the cage and defined the cage plane, thus measuring cage motion for the remaining degrees of freedom (also shown in Figure 7 are the three rear oil jets).

The actual Bently transducer was a flat coil of wire, located on the end of a 0.190 inch diameter, ceramic tip. The coil was protected by 0.010 inches of epoxy fiberglass which was easily rubbed-off if contacted with the rotating target (several probes were ruined during adjustments). Each probe was driven by a RF voltage generated by the proximator (Figure 8). The -18 vdc from the power supply was applied at the proximator input terminals. The proximator (actually a modulator-oscillator) converted this voltage into an RF signal which was applied to the probe through coaxial cable. The probe coil radiated this signal into the surrounding areas as a magnetic field. When the conductive



Figure 7. Pre-amplifier and Power Supply

surface approached the probe tip, eddy currents were generated on the surface of the material and power was absorbed. As the surface came closer to the probe tip, more power was absorbed until the gap was about 0.015 inches when maximum power was lost (saturation). As shown in Figure 9, the proximator measured the RF voltage envelope and provided a DC signal output equal to the negative peaks of the envelope (demodulation). These probes had a scale factor of about 200 mv per 10^{-3} inches and a linear range between 25 and 75×10^{-3} inches. Figure 10 shows the "de-biasing" circuit used to remove the probe signal carrier voltage so that the smaller, dynamic portion of the signal could be more easily observed on the oscilloscope.

Probe temperature affected slightly the range limits of the probe. For this reason, the signals were recorded when the test rig temperature had stabilized. During the experimentation the temperature of the test bearing outer race was between 250 and 300°F causing an increase of the probe signal to be about 1 VDC from the room temperature signal. This was accounted for during the reading of the calibration curves.

The location of the three proximity probes mounted in the shaft axial direction was not adjustable once the test bearing was placed as was possible with the two radial probes. Care was also necessary for maintaining the seal on the back plate to prevent oil leakage out of the test bearing chamber. Therefore, a flexible holder using a bellows spring was designed and fabricated (Figure 3, Letter O). This holder had a stop-pin that touched against the outer ring and allowed precise positioning of the probe from the cage surface.

Figure 11 shows the initial operating locations of the probes. Since the radial probes were effectively less sensitive than the axial probes because of the reduced width of the "target" surface, it was necessary to set them with a smaller clearance so that they were in the linear range of the probe sensitivity. The radial probes were mounted 22.5° off the true inertial z and y axis because of the lack of assessability to the test bearing in the z (vertical) direction

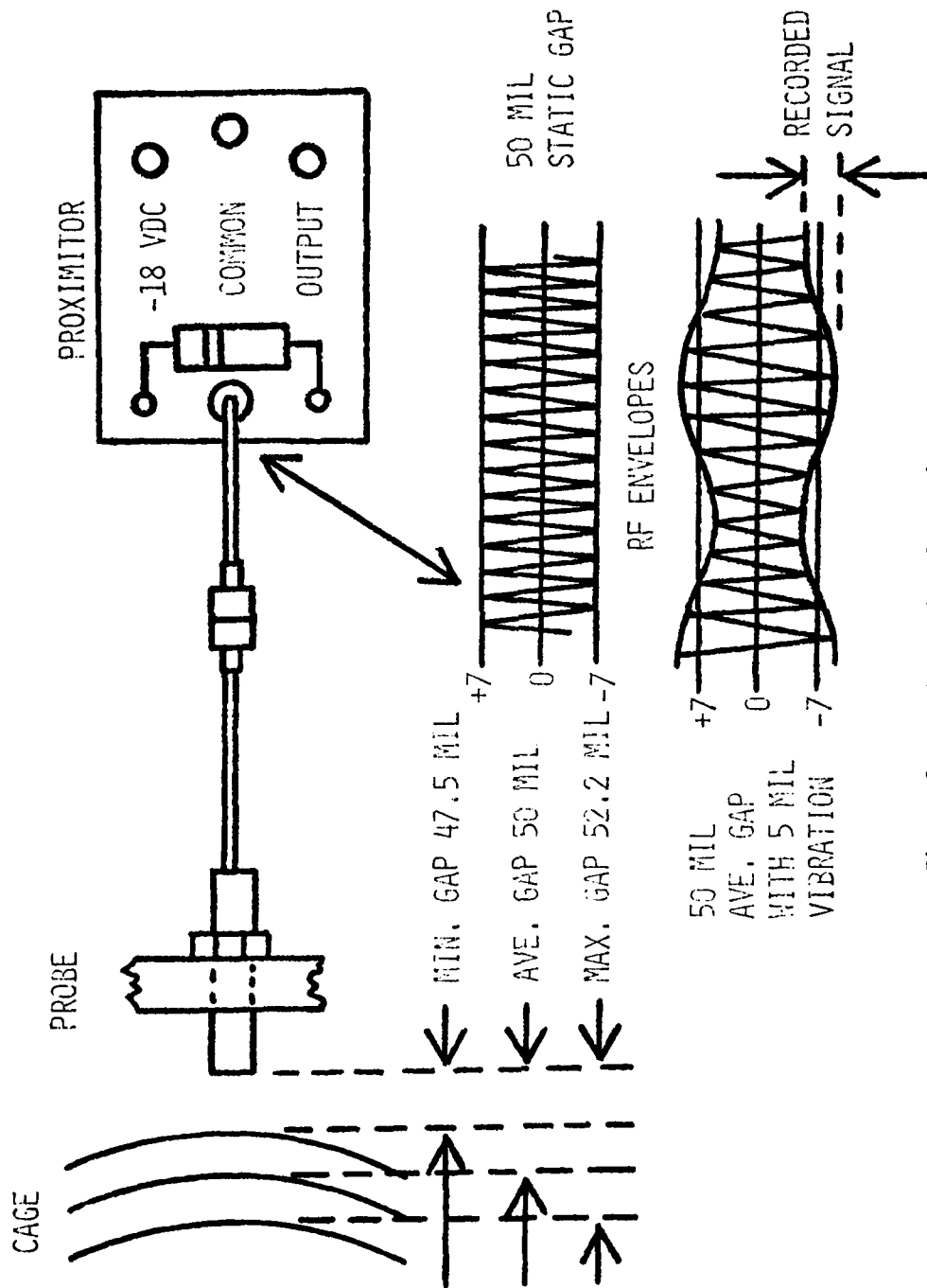


Figure 9. Probe System Operation

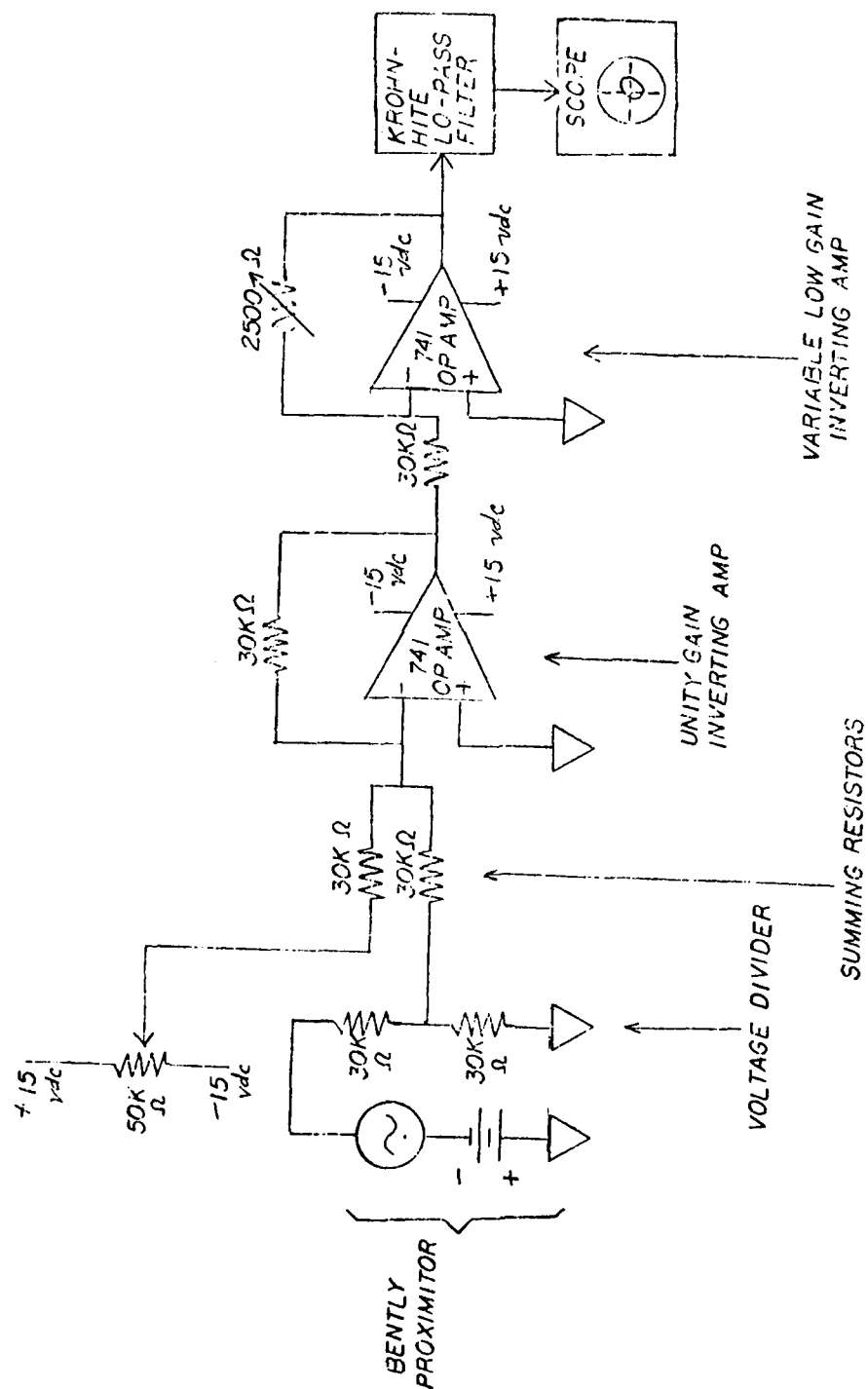


Figure 10. Probe Signal "De-biasing" Circuit

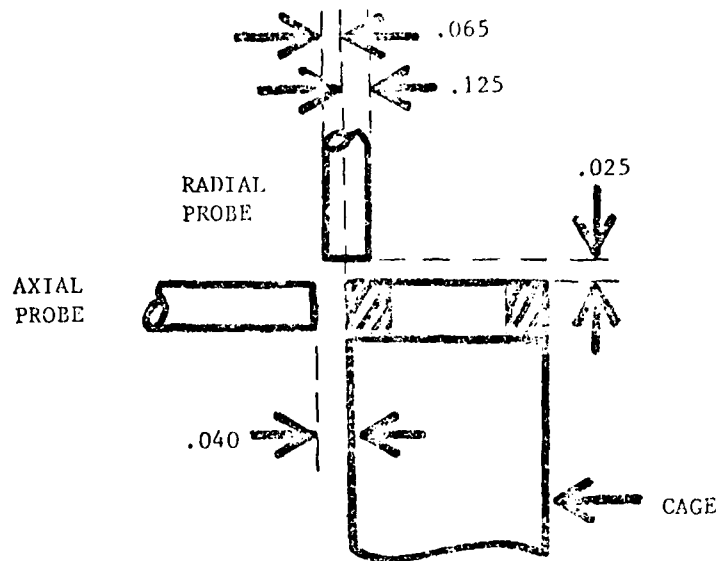


Figure 11. Initial Clearances of Probes

(this was the location of the lubricant supply line). The three axial probes were spaced between the three lubricant jets. Unfortunately, probes #1 and #4 were in close proximity to each other so that during testing it was necessary to turn one of them off while the other was recorded. Otherwise, very "garbled" signals were obtained from both probes.

The probes were extremely sensitive to all discontinuities within the conical range of the emitting tip, as well as all the frequencies associated with cage whirl, ball passage, shaft rotation and others. Therefore, the probe signals were also passed through a narrow band pass filter which allowed selection of the size and location of the frequency "window" to be observed. These signals were fed into a spectral analyzer to provide a dynamic history of the desired frequencies in all three bearing axes.

The probe signals were affected by the orientation, size and conductivity of the target. The 4340 steel cage in the test bearings had a slightly lower conductivity than the M-50 balls and rings. The higher conductive materials consumed less power at a given gap and produced a higher voltage output at the proximator. In addition, the probe target width should ideally be at least twice the diameter of the probe tip, which was not the case for both the axial and radial probes. These factors were accounted for by the calibration scheme described next.

To calibrate the proximity probes, the test bearing head assembly was removed from the bearing rig and mounted on the headstock of a machine lathe. The test bearing inner ring, cage and balls were held together with shim-stock and non-conductive tape and mounted on the lathe tailstock so that the assembly could be adjusted axially and radially with respect to the test bearing head by adjustment of the carriage controls. The five probes were mounted in the test head in same location as during actual test conditions (Figures 12 and 13). Because of the cable leads from the probes, the bearing head was only allowed about one full turn of rotation. Using this set-up, the bearing

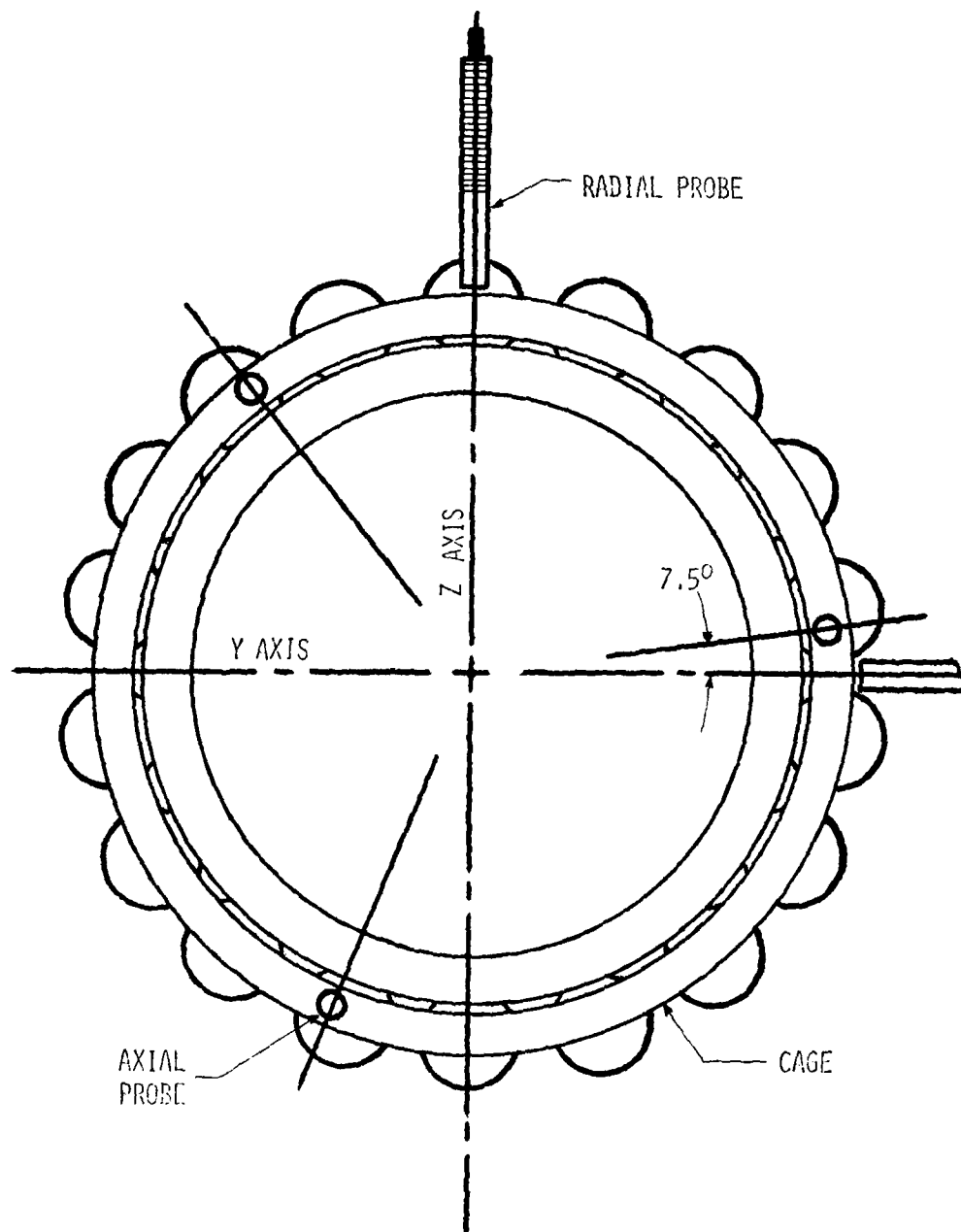


Figure 12. Axial View, Probe Locations (Outer Ring of Peering not Shown).

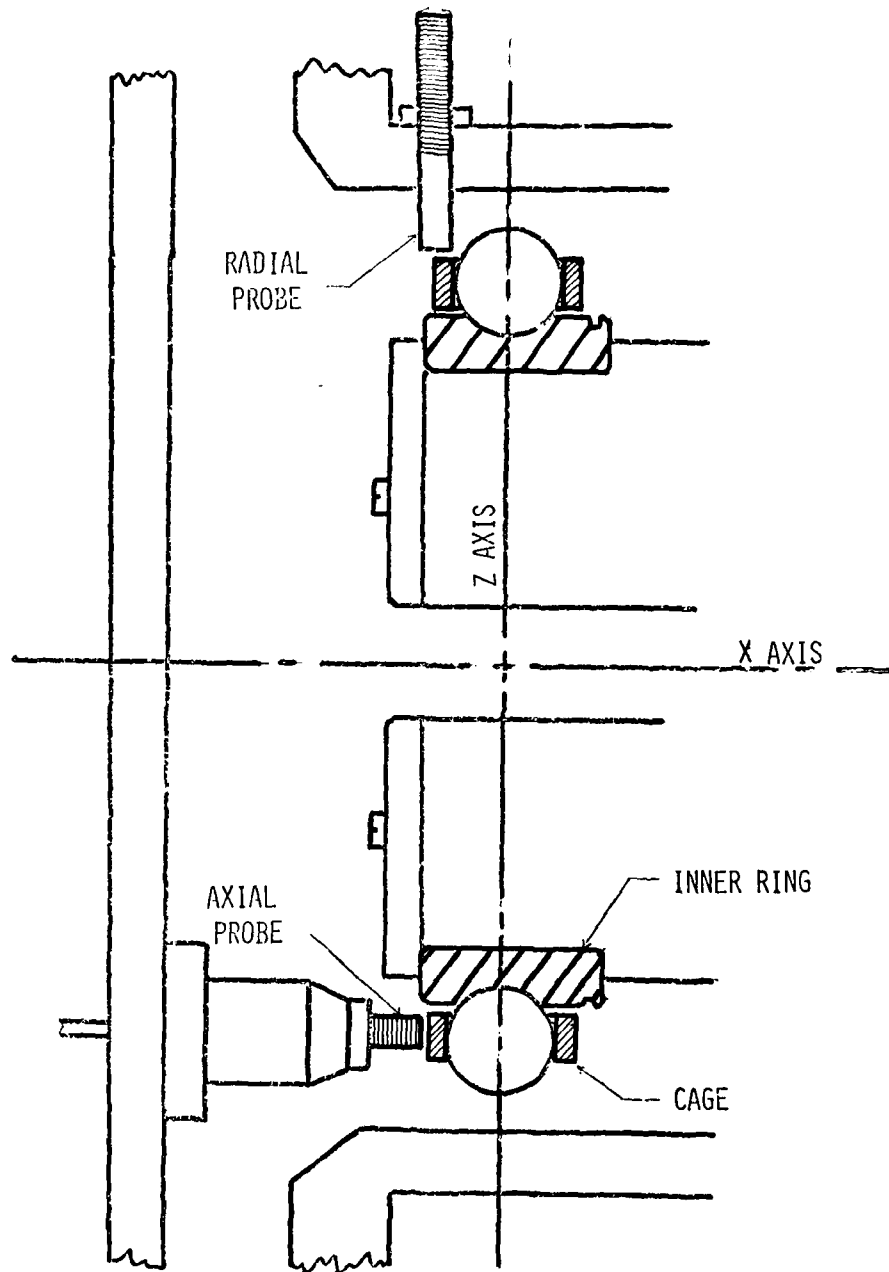


Figure 13. Radial View, Probe Locations (Outer Ring not Shown)

cage assembly was located precisely with respect to the five probes, the signals of which were recorded simultaneously. This data was used to produce a family of calibration curves (Figure 14) for the probe system. The correct radial probe curve was selected based on the axial probe reading.

The calibration of the thrust and torsion strain gage bridges were routinely achieved by the application of known static loads and moments to the shaft. By recording the transducer signals, the calibration curves were obtained. Unfortunately, an uncertain amount of coupling existed between the thrust and torsion bridges. Compensating for the effect of test bearing thrust loads on the output for the torque bridge was done by calibrating the output of this bridge as a function of the thrust loads applied to the shaft. This calibration was then subtracted from the total output of the torsion bridge during testing, the amount subtracted determined by the test thrust load.

2. EXPERIMENTAL PROCEDURE

Although the two bearing models, DREB and SHABERTH, had different areas of sophistication, they each computed certain fundamental parameters of bearing performance which could be compared either together or separately against the experimental data. The experimental data acquisition was accomplished in two phases, labeled for simplicity as the "parametric study" and the "dynamic study."

a. Parametric Study

To obtain the experimental values of three parameters (torsion, heat generation, cage orbital speed) several runs on the bearing test rig were conducted during a period of many months. The test bearing was repeatedly subjected to a predetermined series of nominal loads and shaft speeds which were simulated by the mathematical models.

The tests consisted simply of first applying the axial thrust load to the test bearing by supplying pressure from the nitrogen gas bottle

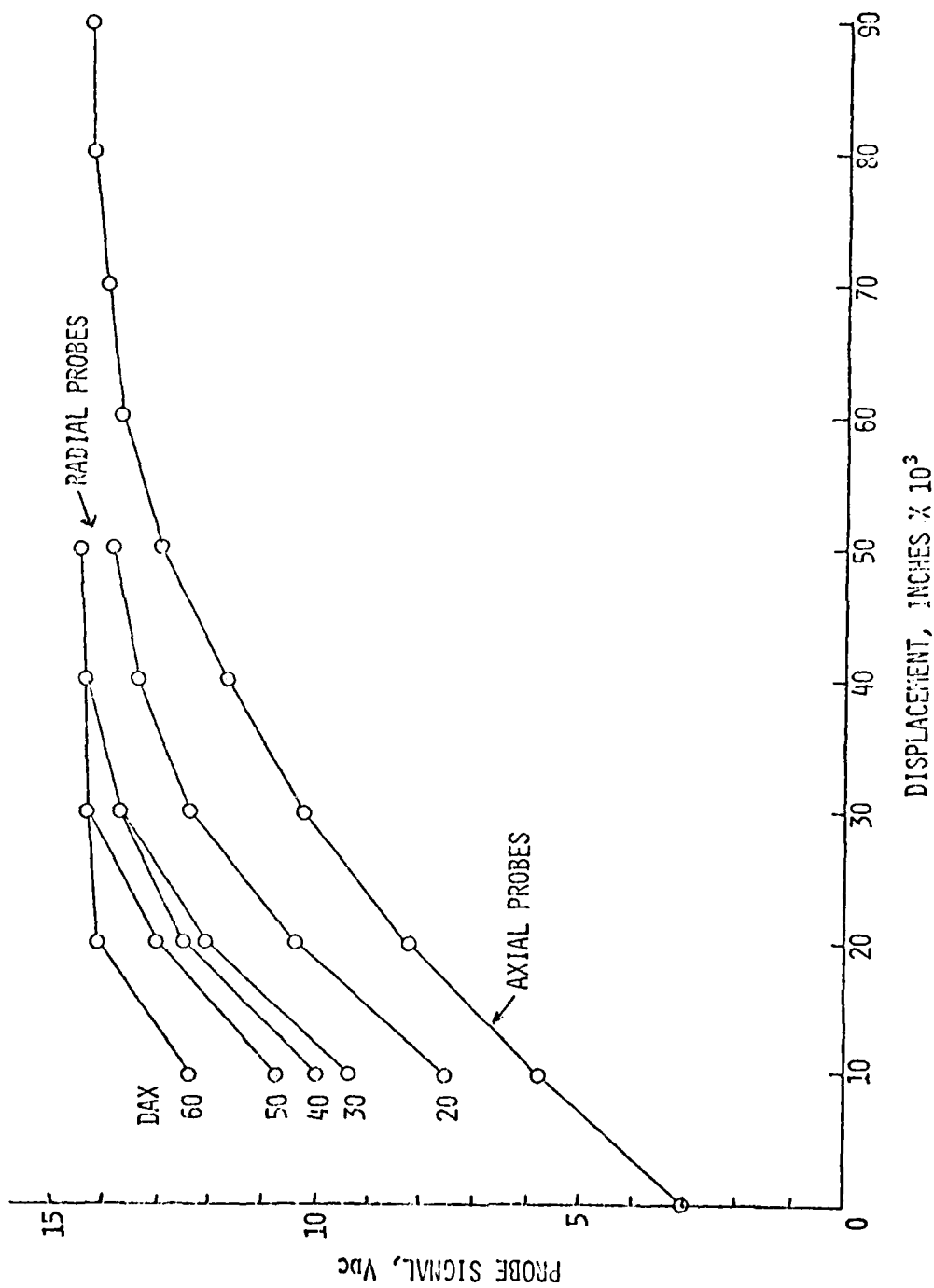


Figure 14. Proximity Probes Calibration Curves (Showing Variation of Radial Probe Sensitivity with Axial Position of Cage)

to the loading diaphragm. This force was measured to within 100 lbf by using the strain-gage transducer and the calibration curves. For the constant thrust load, data for the entire range of shaft speeds was recorded before increasing the load to the next value. The speed was not increased, however, until the test rig and lubricant had warmed to a stable level, as indicated by the temperatures at the inner and outer rings, the support bearing, and the oil supply and sump locations. This usually required operation for one to two hours. The approximate temperatures reached were the following:

Inner Race - 280°F	Oil Supply - 280°F
Outer Race - 300°F	Oil Sump - 280-310°F
Support Bearing - 160°F	

Since it was known that the quantity and temperature of the test bearing supply lubricant affected significantly the performance of the bearing, the lubricant was supplied at a constant rate of 2 (+0.2) gal/min and at a temperature of about 280°F. This range was maintained by circulating the lubricant from the test bearing sump through a heat exchanger cooled with tap water.

The experimental value for torsion of the bearing exerted on the shaft (rolling-resistance) was obtained by measurement of strain from the torsion transducer used in conjunction with the calibration curves. These torque values were recorded for later comparison to the values predicted by DREB and SHABERTH.

The experimental cage orbital speeds were obtained using an axially mounted proximity probe and a special cage fitted with three evenly spaced pins. The three-per-revolution impulse was transformed by a digital counter to the measured value for cage orbital speed. The values were recorded for later comparison to the speeds calculated by DREB and SHABERTH.

SHABERTH predicted a total heat generation rate which was compared to the lubricant mass flow heat transfer rate of the experiment. This rate was approximated by multiplying the temperature difference of the lubricant between the supply and the sump locations by the mass flow of the lubricant (2 gal/min) and the approximate heat transfer coefficient ($C_p = 0.54 \frac{\text{BTU}}{\text{LBMF}}$). Because an uncalculable amount of energy was dissipated to the test rig and surrounding atmosphere, this heat generation rate was expected to be less than the total rate predicted by SHABERTH.

b. Dynamic Study

In order to ascertain the validity of the predictions provided by the DREB dynamic analyses, a series of dynamic tests were conducted on the bearing test rig. These tests consisted essentially of measuring the output of the Bently probes on either the frequency spectrum analyzer or the oscilloscope for the various load-speed conditions.

1) Lissajous Tests

Lissajous figures depicting the cage imaginary mass center whirling motion were obtained by use of the two radial, Bently probes. Their signals were treated with a low-pass filter set slightly higher than the 1/rev shaft frequency primarily in order to remove the ball pass frequency. The signal carrier voltage was removed so that the oscilloscope sensitivity could be increased to observe the dynamic portion of the DC signal. The two radial probe signals were coupled by inputting the vertical radial probe to one channel and then connecting the horizontal probe to the external horizontal input of that channel, replacing the time sweep. Care was taken to insure that the sensitivities in both axes were equal.

In order to obtain a direct physical interpretation of the image made on the scope graticule by the radial probes, it was necessary to locate the true shaft/bearing center on the scope graticule. To do this, the test rig was partially disassembled to provide access to the test bearing. The test bearing cage was then physically centered on

the shaft by wedging .010 inch shimstock into the clearance between the cage and the inner race, which was assumed to be concentric with the shaft axis. The scope x-y position controls were then adjusted until the signal point from the coupled probes was centered on the scope display graticule. The shimstock was removed and the test rig was reassembled. Unfortunately, during assembly the cage axial position had shifted, thus changing the Bently probe sensitivity and causing the point signal to move off the scope graticule.

The next attempt to center the shaft center on the scope graticule was based on the fact that the cage was supported by the inner ring. With no shaft revolution the clearance between the cage and the top (+z) position of the inner ring was assumed to be zero. Also the clearances at the horizontal (-y, +y) positions were assumed to be equal presuming the balanced cage was indeed hanging freely on the inner ring. With the test rig assembled, the point signal from the coupled radial probes was centered horizontally on the scope graticule and positioned halfway between the graticule center and the maximum vertical signal displacement. The test rig motor was turned on and then engaged and disengaged with the shaft several times to see if the point signal would always return to the pre-set center. This would indicate that the cage had returned to its original position. It did for about 70% of the trials but it was concluded that the true center position on the scope graticule could not be found with complete accuracy. For low shaft speeds (about 100 rpm), however, the whirl ellipse consistently found the same location on the graticule so it was decided to use this location as the reference starting point. After the rig had been allowed to warm-up for several hours, the Lissajous figures were photographed for loads ranging from 500 to 4,000 lbf and speeds from 2,000 to 15,000 rpm.

Because the shaft center could not be accurately centered on the scope graticule, and because only the dynamic signal from the probes was observed, the absolute magnitude of displacement of the cage center from the shaft center was not determined using the Lissajous figures. Nevertheless, a change in location of the cage center was measurable

and comparable to the trends predicted in the DREB analysis. The photographed figures also displayed the shape, orientation, and size of the cage mass center orbit which were compared to the DREB prediction for cage radial position.

The Lissajous figures were also used to find the cage-inner race contact angle (sometimes referred to as attitude angle) made by the inertial z axis and the line of minimum film thickness between the cage and the inner ring. This angle was measured from the z axis in the direction of shaft rotation and compared to the DREB calculated values.

2) Frequency Spectrum Tests

The five Bently probes were used with a spectral analyzer to obtain a three-dimensional representation of the cage dynamics during bearing operation. The amplitudes of the cage oscillations were recorded for comparison to the DREB analysis for cage position versus time. This data also provided a better understanding of the torsion and heat generation values as obtained in experiment and as calculated by DREB and SHABERTH.

The signals were filtered to a frequency range which contained the cage and shaft orbital frequencies, but not the ball-pass frequencies. The thrust loads and shaft speeds were applied to the test bearing in the same manner as for the Lissajous study. The display of the frequency spectrum was recorded on an x-y plotter for each case and for both radial probes and at least one axial probe.

SECTION IV

RESULTS

1. COMPARISON OF ANALYTICAL DATA WHICH WERE NOT MEASURED IN THE EXPERIMENTAL PHASE

Three important parameters describing the ball-race contacts were not measurable in the experimental set-up. The comparison of contact angles, contact stresses and EHD film thickness as calculated in DREB and SHABERTH was performed to examine their effects on calculated fatigue life and cage orbital speed. This comparison discussed next helped in the evaluation of the usefulness of the two models.

a. Stress and Angle of Ball-Race Contact

A comparison of DREB and SHABERTH predicted values for contact stress between a ball and the two races is shown in Figures 15 and 16. The magnitudes of the predicted stress levels were essentially equal for both programs demonstrating a similarity between their static equilibrium routines. For increasing shaft speed, the inner race contact stress decreased as the outer race stress increased. This was due mainly to the increased centrifugal loading of the balls on the outer race. In fact at some high speed the outer race stress would surpass the inner race stress, although this was not observed for the range of speeds in this study. A relation between contact angle and contact stress could be observed in both programs. Figures 17 and 18 show that the ball-outer race angle decreased greatly with increasing speed while the ball-inner race angle increased gradually with increasing speed. This was also an effect of the ball centrifugal forces. A decrease in contact angle caused an increase in stress for either race, a result of an increase of the normal load vector at each contact.

b. EHD Film Thickness at Ball-Race Contacts

The EHD film thickness calculated by DREB and SHABERTH are shown in Figures 19 and 20. For both the inner and outer race contacts, the

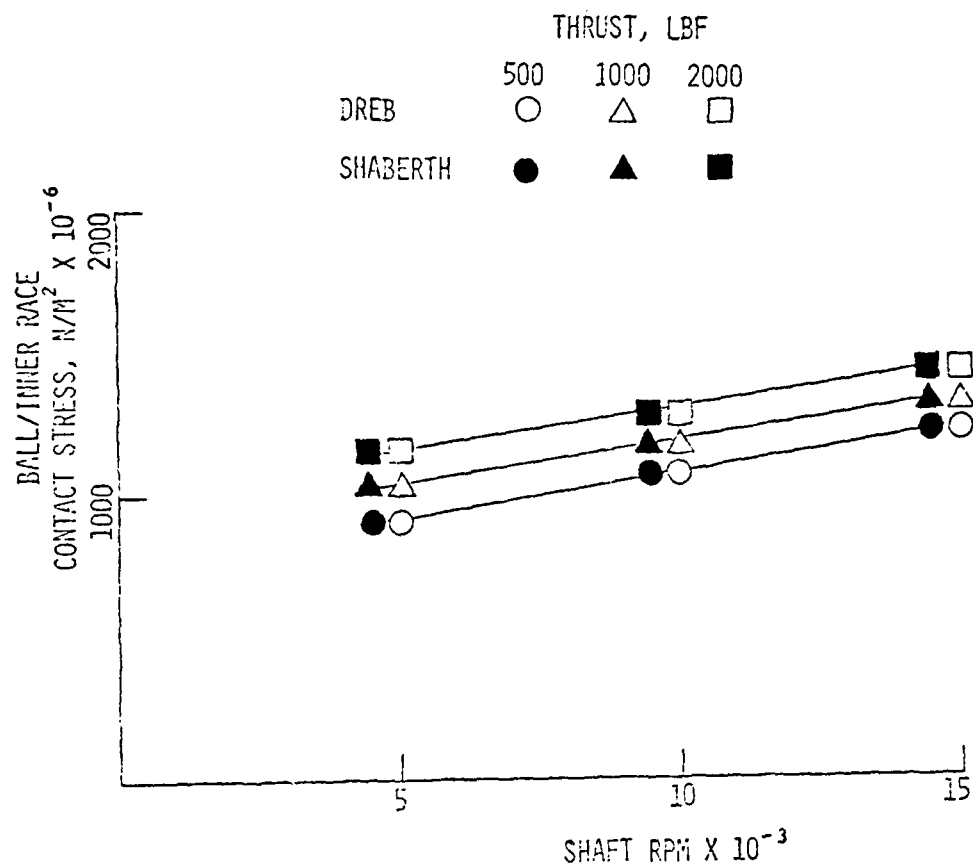


Figure 15. Ball-Inner Race Contact Stress

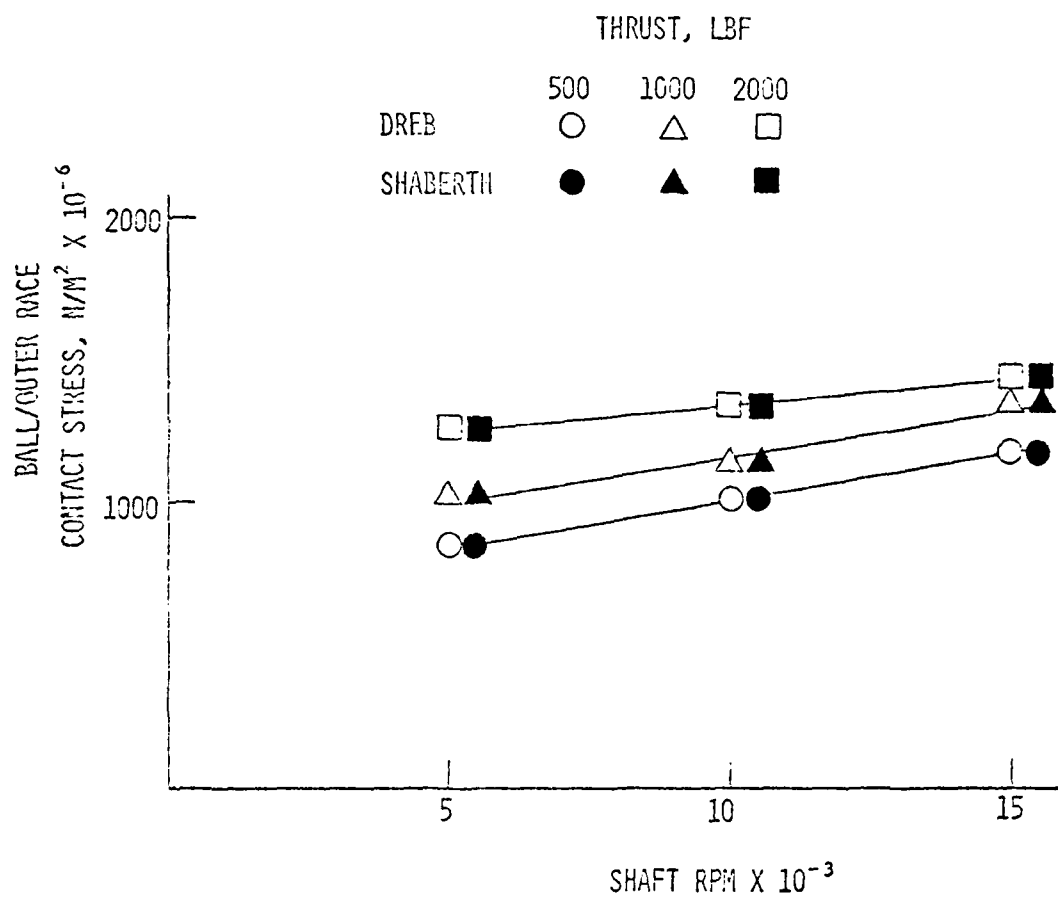


Figure 16. Ball-Outer Race Contact Stress

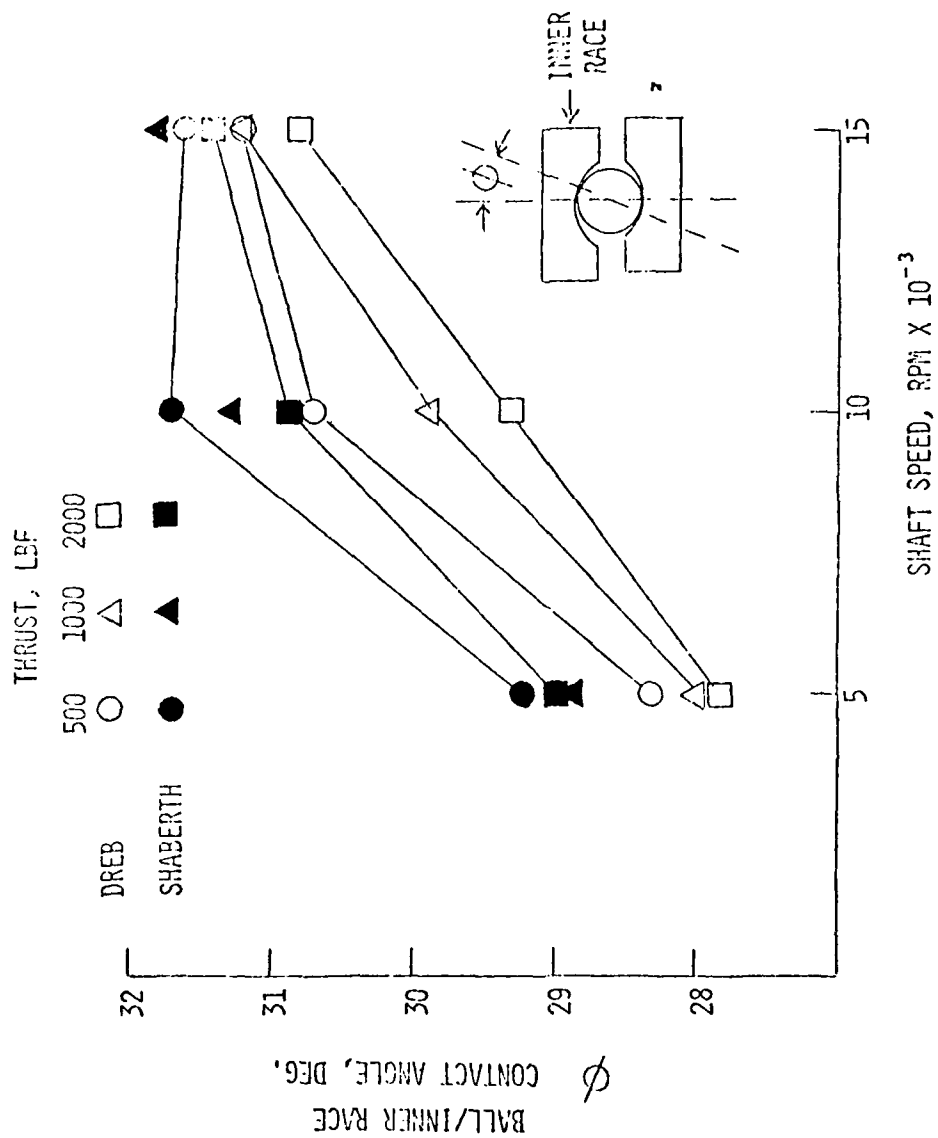


Figure 17. Ball-Inner Race Contact Angle

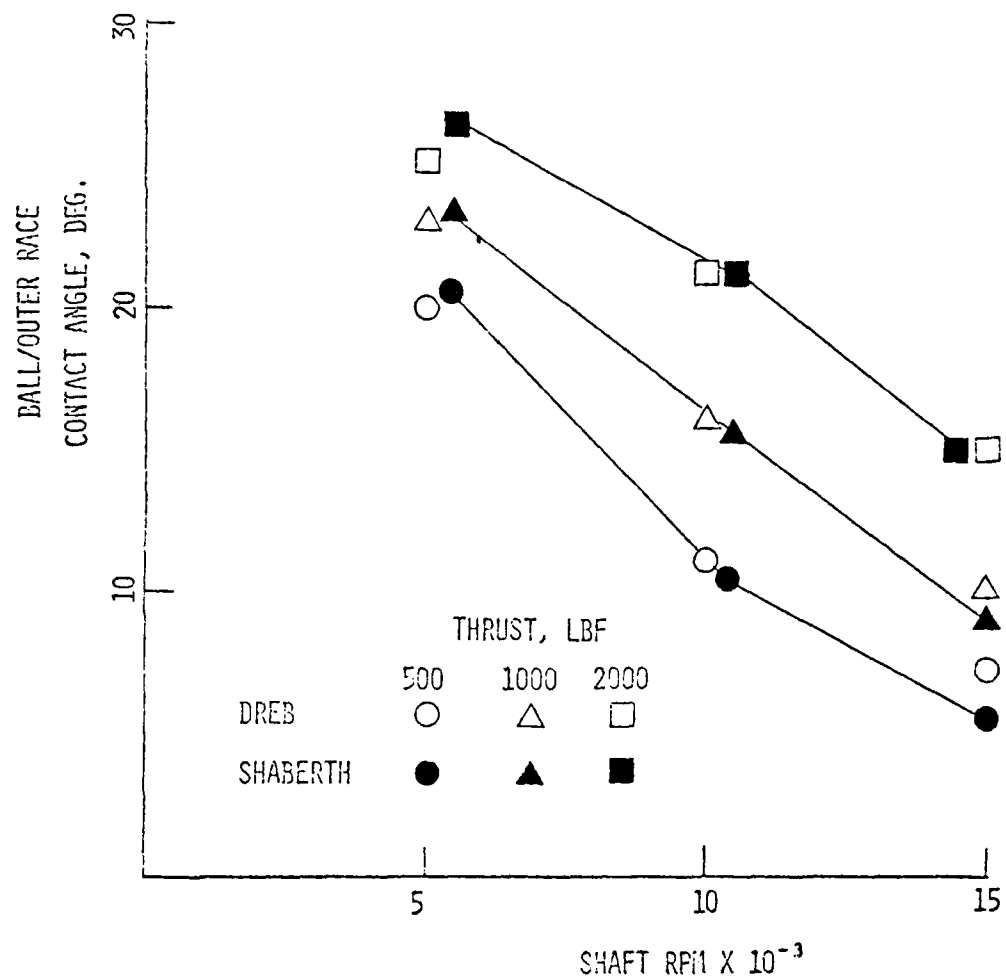


Figure 18. Ball-Outer Race Contact Angle

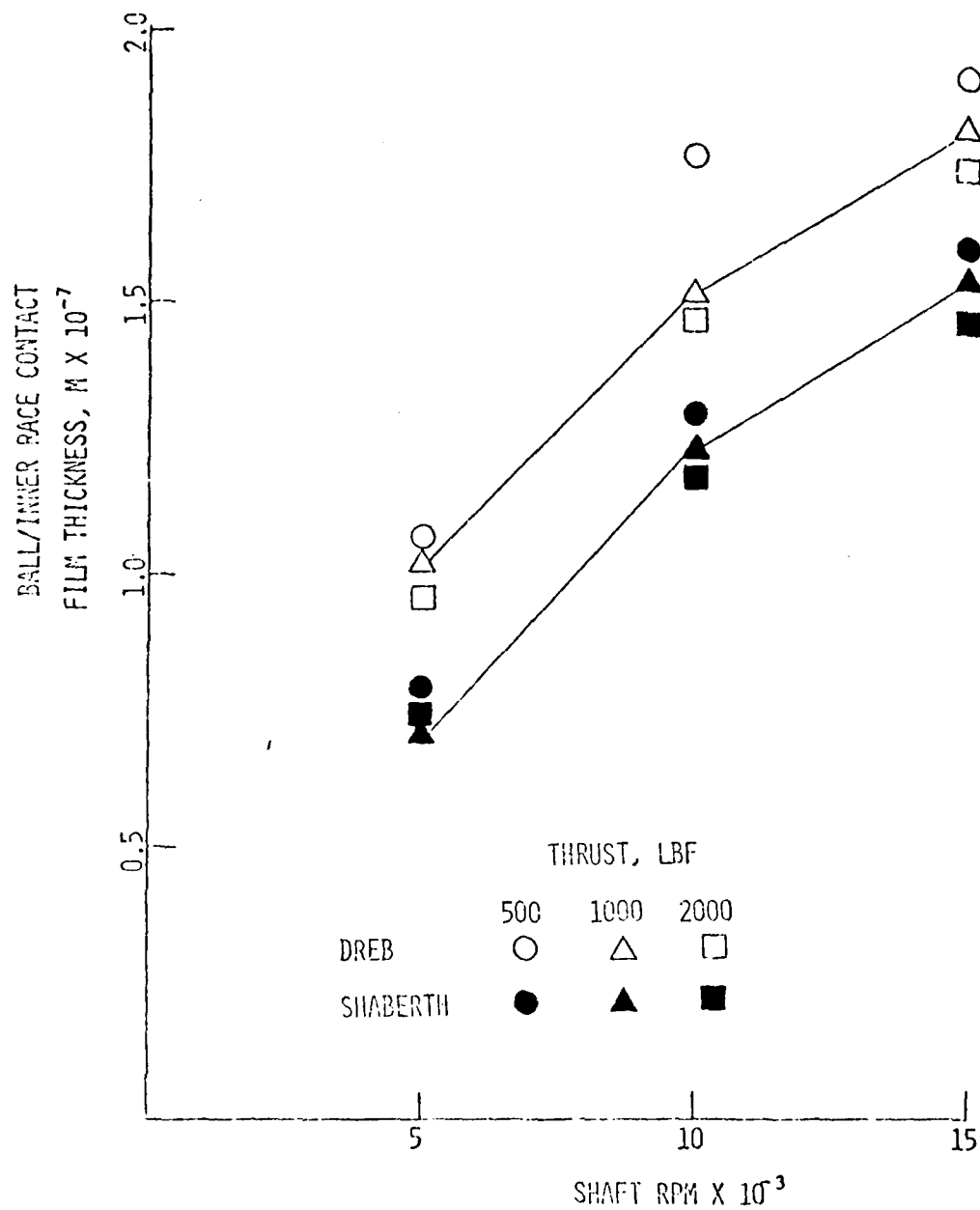


Figure 19. Ball-Inner Race Contact Film Thickness

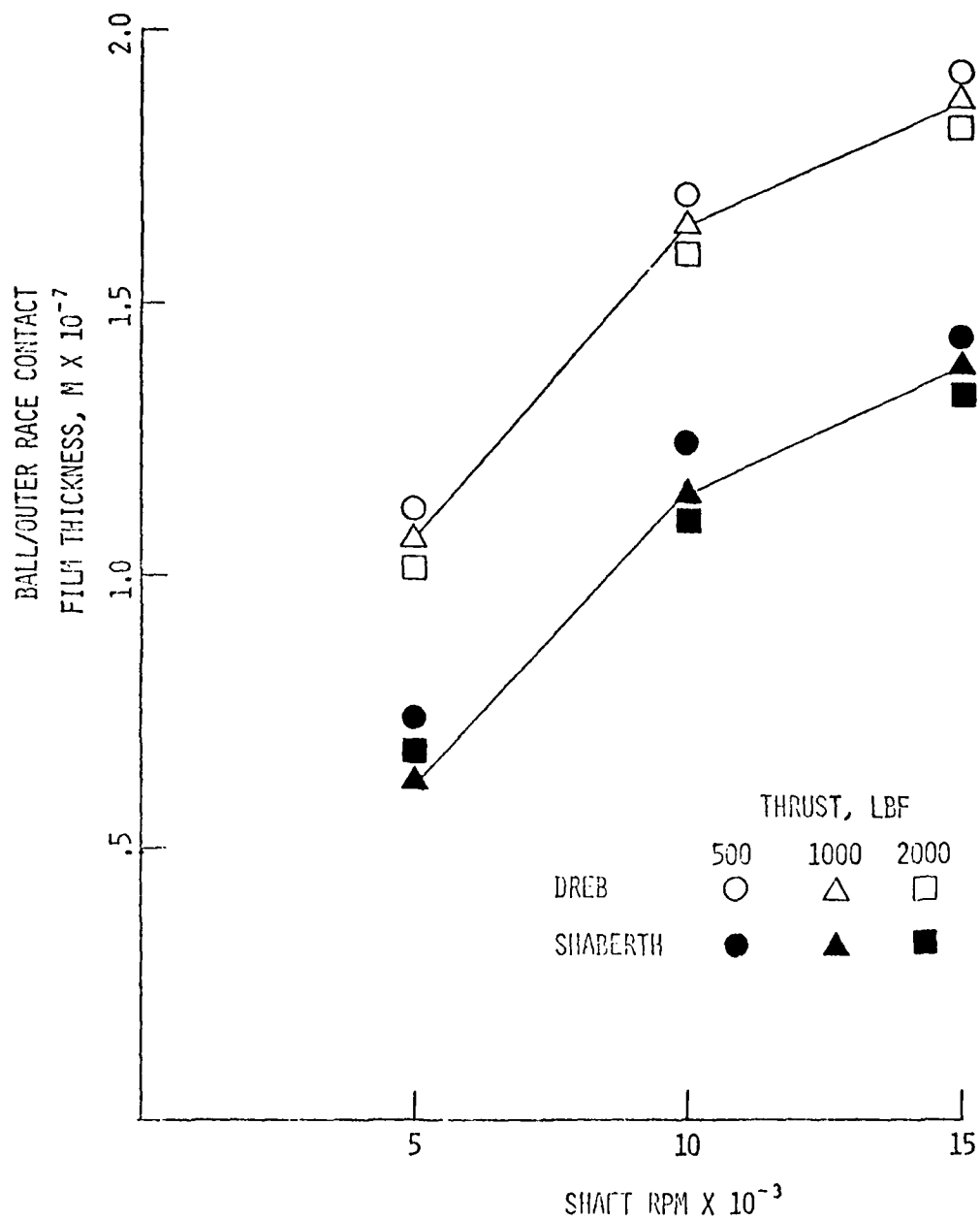


Figure 20. Ball-Outer Race Contact Film Thickness

DREB values were notably higher (as much as 30% higher) than the SHABERTH values exemplifying their differing theoretical basis. Both models show the steepest increase of film thickness between 5,000 and 10,000 rpm and then more gradual increases thereafter for increasing speeds.

Note that the contact stresses calculated by DREB were essentially equal to those from SHABERTH, despite the differences in film thickness. The normal force transmitted through the EHD contact and the area of the contact zone was independent of the thickness of the film. Actually the film thickness is a function of the load and the contact zone area is a function of the conformity and elasticity of the contacting bodies.

c. Fatigue Life

The DREB and SHABERTH values for L10 fatigue life for the total bearing are shown in Figure 21. Because of the long fatigue life of this bearing, a statistically meaningful experiment for determination of actual life could not be conducted in a reasonable time frame. Therefore, no experimental fatigue data was obtained. Also no other endurance life data obtained by other investigators for this particular bearing configuration was available.

Figure 21 shows a decrease in predicted life with an increase in load and shaft speed. This is due to the increased stress and number of stress cycles per hour for the higher DN cases.

The SHABERTH fatigue lives were generally about twice as high as the DREB values, even though SHABERTH calculated thinner EHD films in the ball-race contact. The application of different material and lubricant life factors by SHABERTH to the basic fatigue life of the total bearing was the reason for the difference from the more conservative values of DREB.

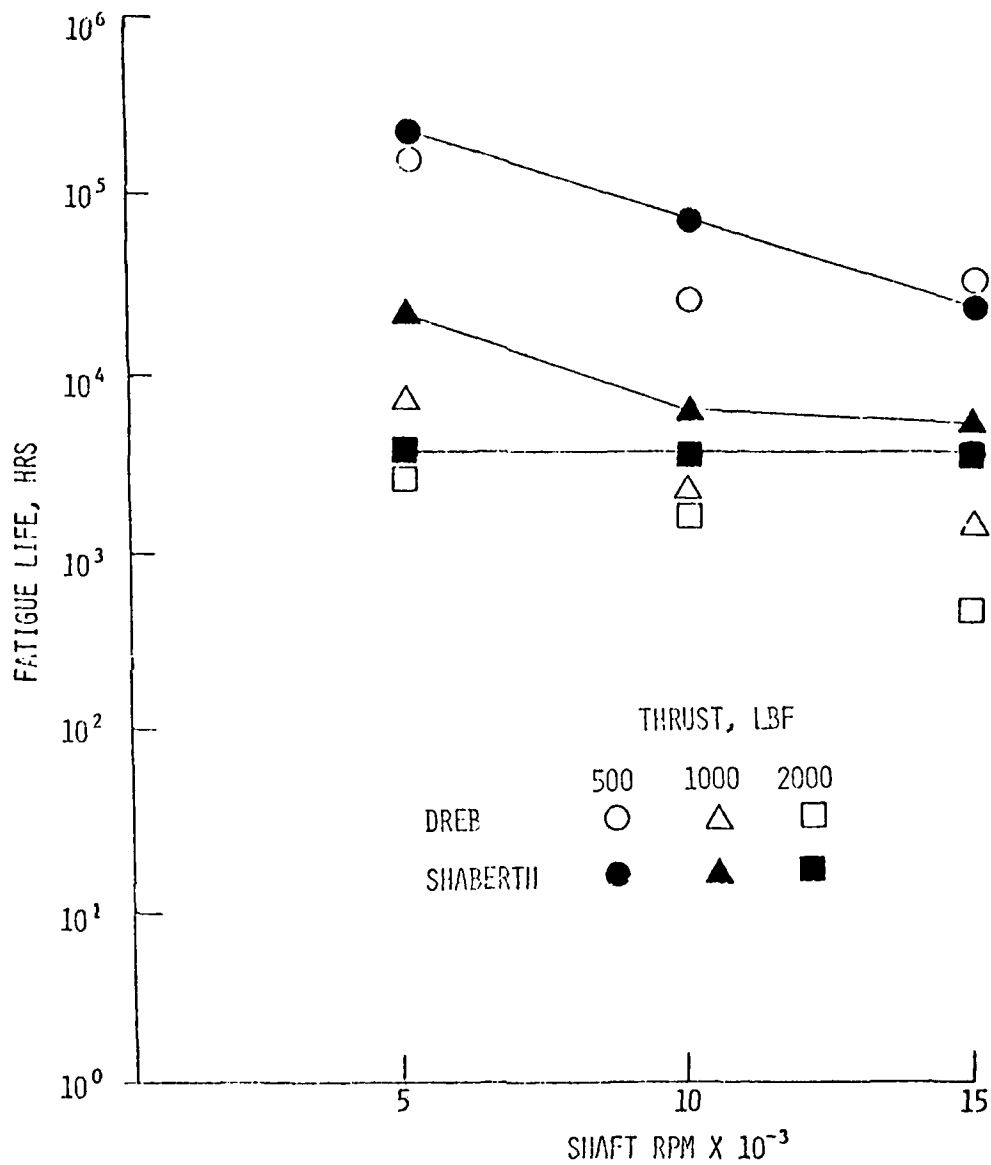


Figure 21. L-10 Fatigue Life (Rolling Contact)

2. COMPARISON OF ANALYTICAL DATA TO THE EXPERIMENTAL
PARAMETRIC STUDY RESULTS

a. Bearing Torque

Figure 22 shows a sample x-y plot of the experimental bearing rolling resistance torque versus time for a thrust load of 1,000 lbf and shaft speeds of 0 to 12,500 rpm. The points shown with this curve are the average values from five curves for the 1,000 lbf case, each of which were recorded during separate tests. The general trend shows increasing torque with increasing shaft speed and vice versa. Also shown in Figure 22 are the SHABERTH predicted values for the total torque.

Throughout the experimentation the torsion sweeps were characterized by a sudden torque decrease during the 5,000-7,000 rpm range. Such a decrease may identify the bearing speeds at which either EHD full-film lubrication is established in the races, or perhaps the formulation of the hydrodynamic lubrication film between the cage and the inner ring.

As shown in Figure 23, DREB predicted total torque values which generally were much higher and more erratic than the SHABERTH and experimental values. It must be remembered, however, that the DREB values shown were time dependent. Figure 24 shows the torque variation with time as plotted by DREBP.

b. Heat Generation

Figure 25 shows the total heat generation rate calculated by SHABERTH compared to experimental lubricant mass flow heat transfer rate. As expected, the experimental value was lower than predicted since it does not account for heat energy dissipated to the test rig and the atmosphere. Nevertheless, it does show order-of-magnitude similarity to SHABERTH values, as well as a deep dip in heat generation for the 5,000-10,000 rpm/region.

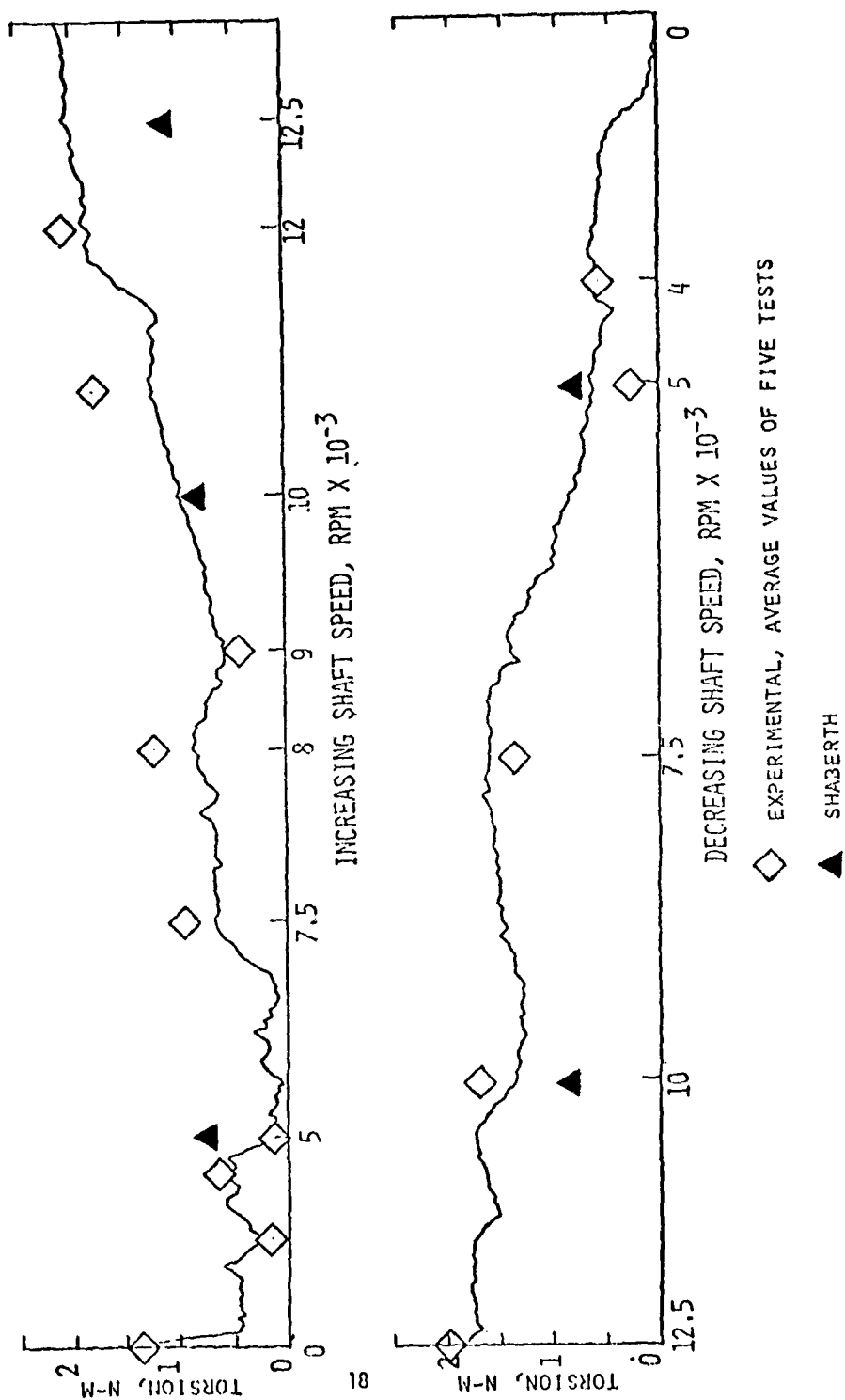


Figure 22. Bearing Torsion, Experimentally-Obtained Sweep for 4448 N Thrust, Shown with SHABERTH values and averaged experimental values

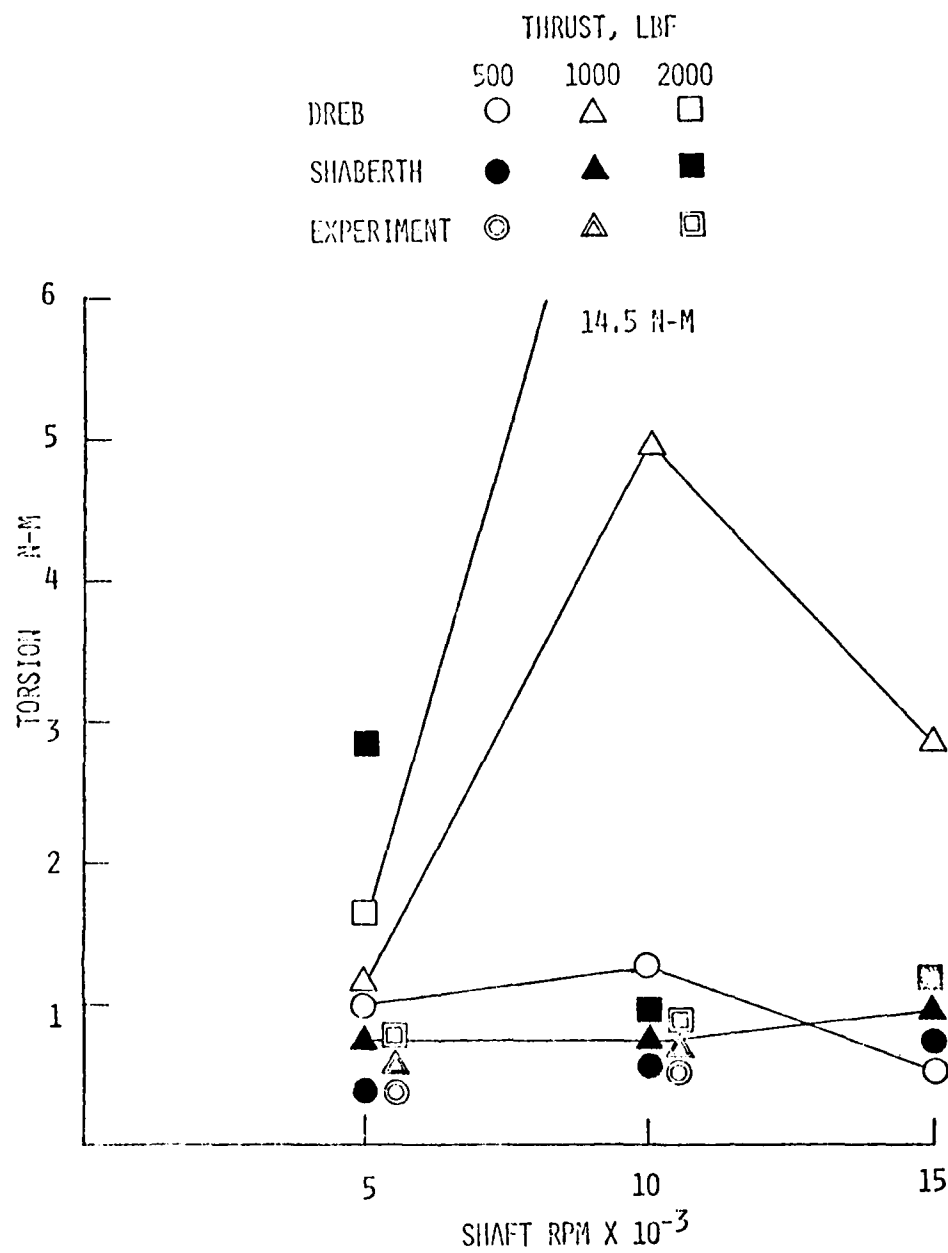


Figure 23. Experimental and Predicted Torsion

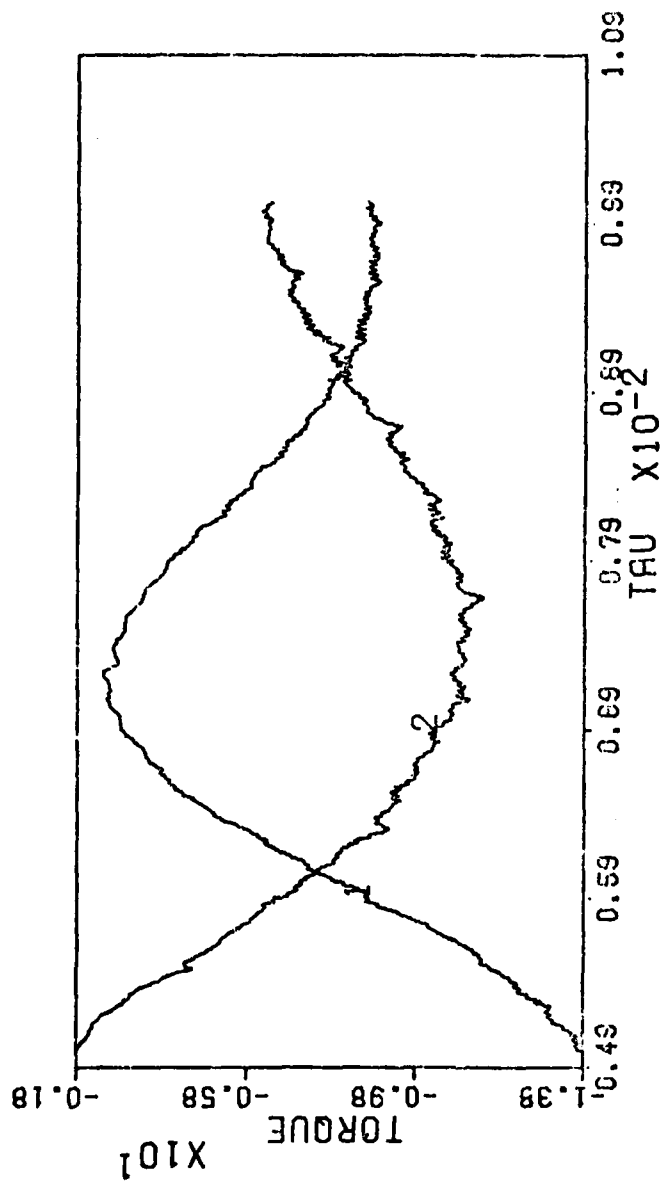


Figure 24. DREBP Plot of Torque Variation with Time

Inner Race = 1

Outer Race = 2

Torque Scale Factor = 84.73 N-m

Time Scale Factor = $1.74 \cdot 10^{-4}$ sec

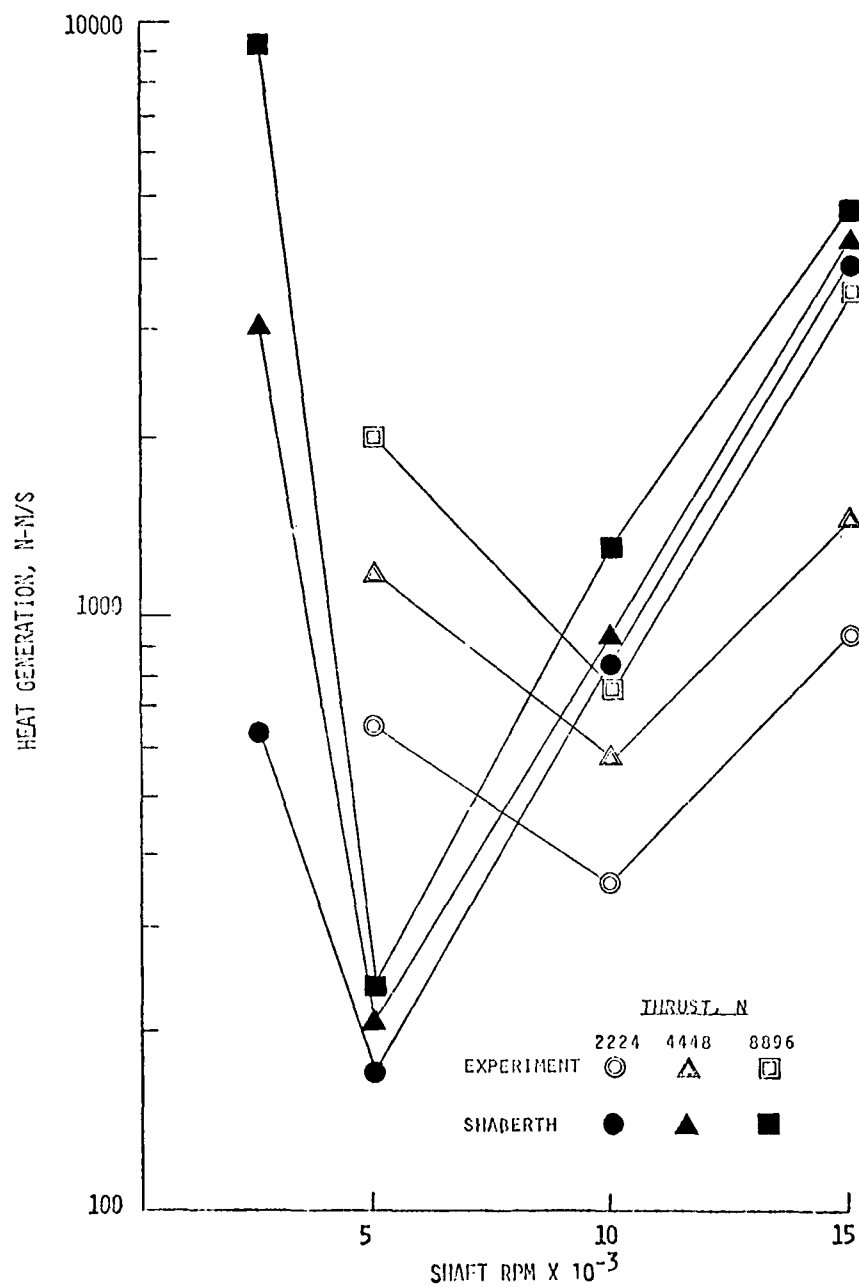


Figure 25. Heat Generation

It was in this same speed range that minimum torque levels were recorded. Probably this information indicates that the establishment of a cage hydrodynamic film or EHD race lubrication or both must have occurred in the 5,000 to 10,000 rpm shaft speed range.

DREB calculated total power loss values are shown in Figure 26. For lower loads, power loss increased linearly with speed. Total power loss was not measured experimentally in this study but since most of the power was lost through heat generation a rough comparison between Figures 25 and 26 can be made. Generally the DREB values seem to increase too rapidly although the values are within realistic limits.

c. Cage Orbital Speed and Skidding

The predictions by DREB and SHABERTH for cage orbital speed are shown with the experimental and epicyclic (solid line) speeds in Figure 27. DREB corresponds with experiment more closely than SHABERTH, although the difference is less than 5%. Variation of the load from 500 to 2,000 lbf apparently had little effect on the cage speed, so only the 500 lbf case is shown in Figure 27. Figure 28 shows the cage speed variation with time as plotted by DREBP. This variation was less than 10% of the cage speed, so the DREB values taken from the 200th time step were used in Figure 27.

3. COMPARISON OF DREB OUTPUT TO EXPERIMENTAL DYNAMIC STUDY RESULTS

a. Lissajous Figure Test Results

Figure 29 shows the experimentally obtained family of Lissajous figures which describe the cage mass center whirling motion in the radial plane. The figures shown are tracings of the actual photographs taken on the oscilloscope. As described earlier, the cross in the center of each box represents the probable shaft/bearing center and the inertial z and y axes were rotated 23.5 degrees counter-clockwise (CCW) to correspond with the orientation of the radial Bently probes. Shaft rotation as it appeared in the oscilloscope was in the CCW direction.

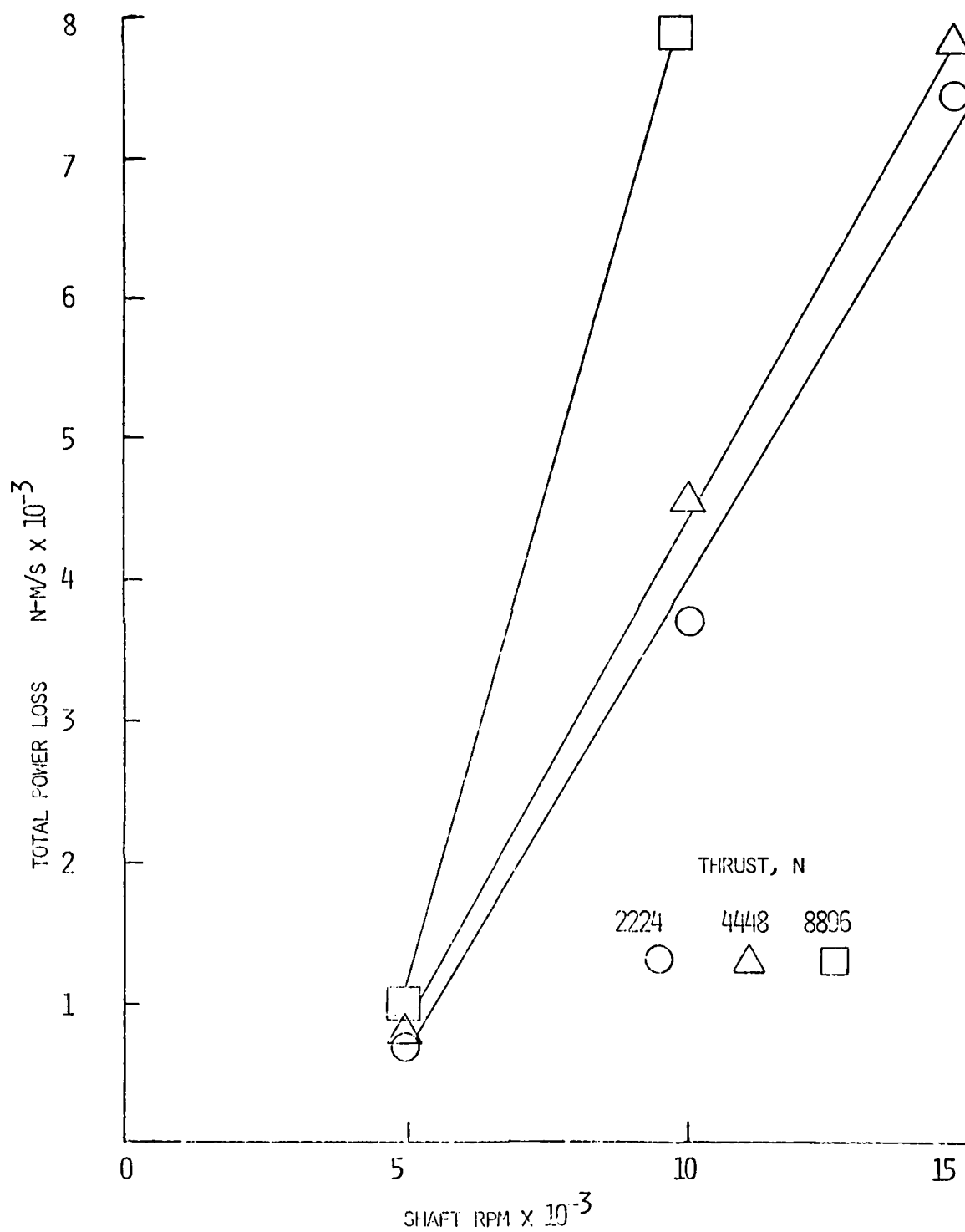


Figure 26. DREB Power Loss

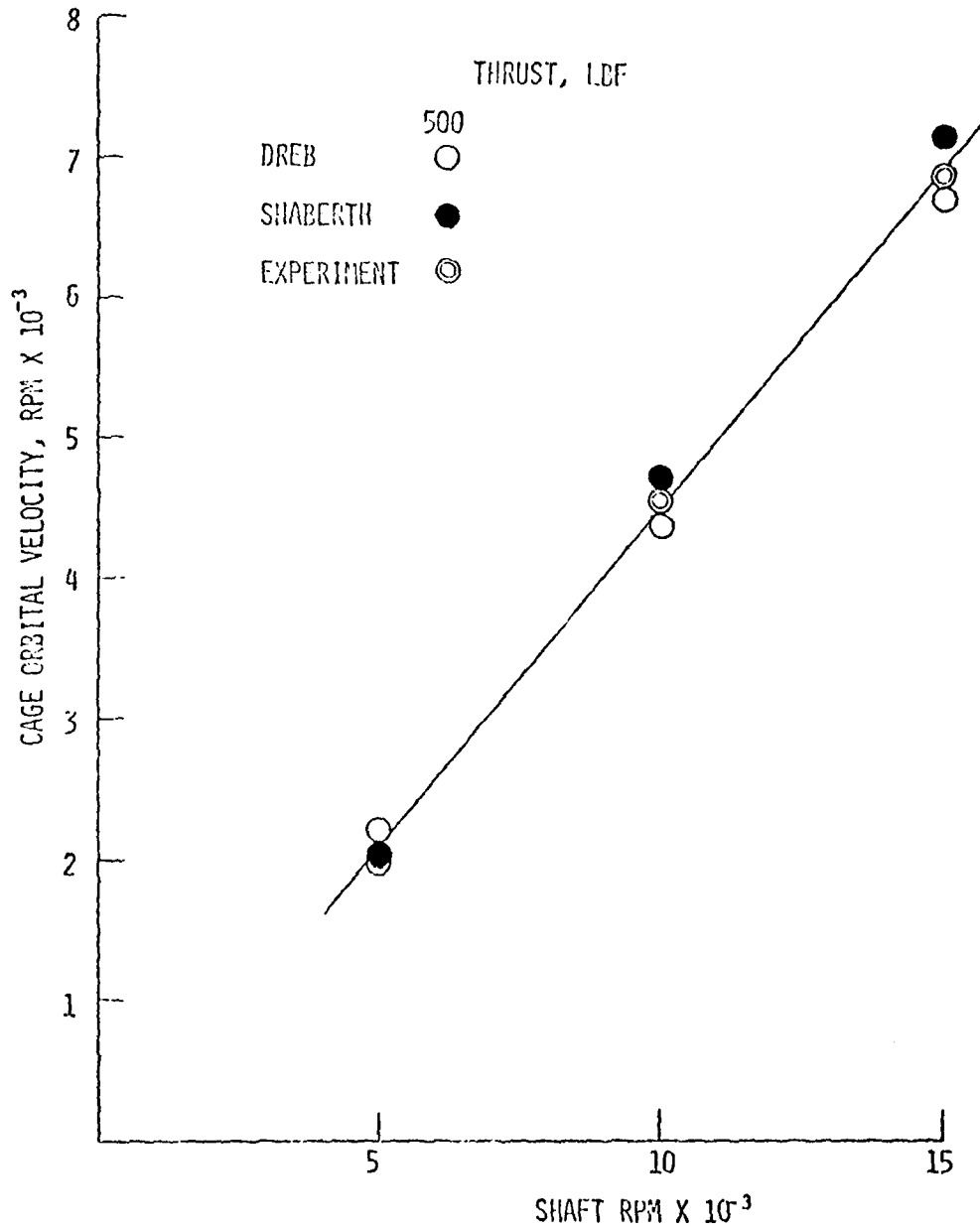


Figure 27. Cage Orbital (Rotational) Speed

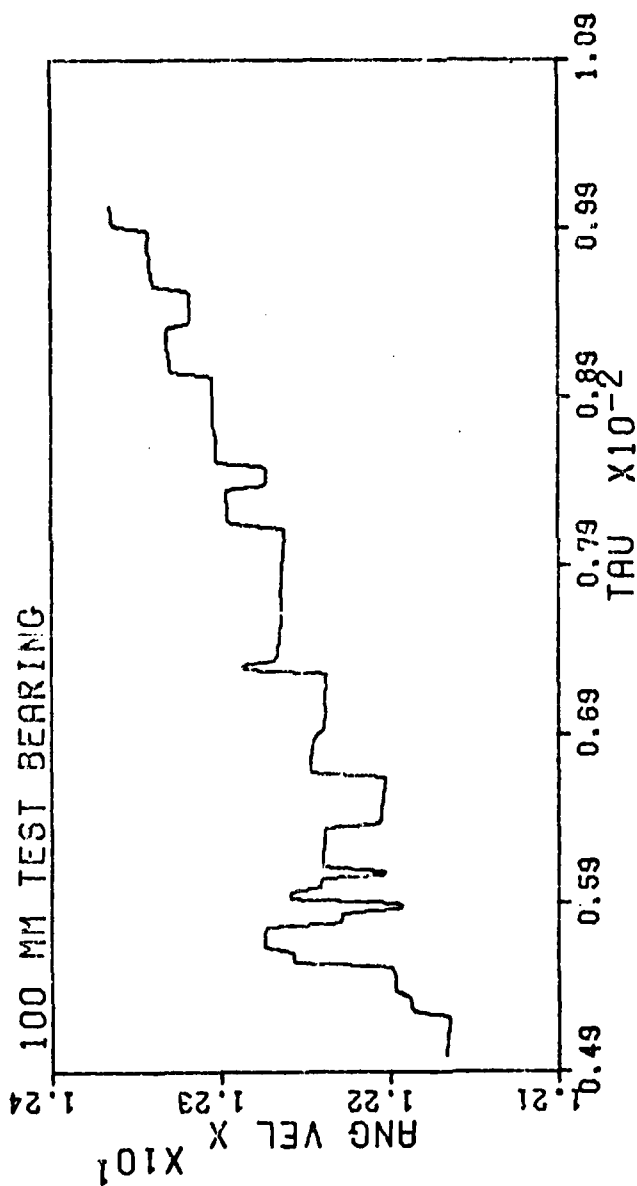


Figure 28. DREBP Cage Orbital Speed Variation with Time
 Shaft Speed = 15,000 rpm
 Velocity Scale Factor = 5.49×10^4 rpm
 Time Scale Factor = 1.74×10^{-4} sec

LISSAJOUS FIGURES OF CAGE MASS CENTER ORBIT

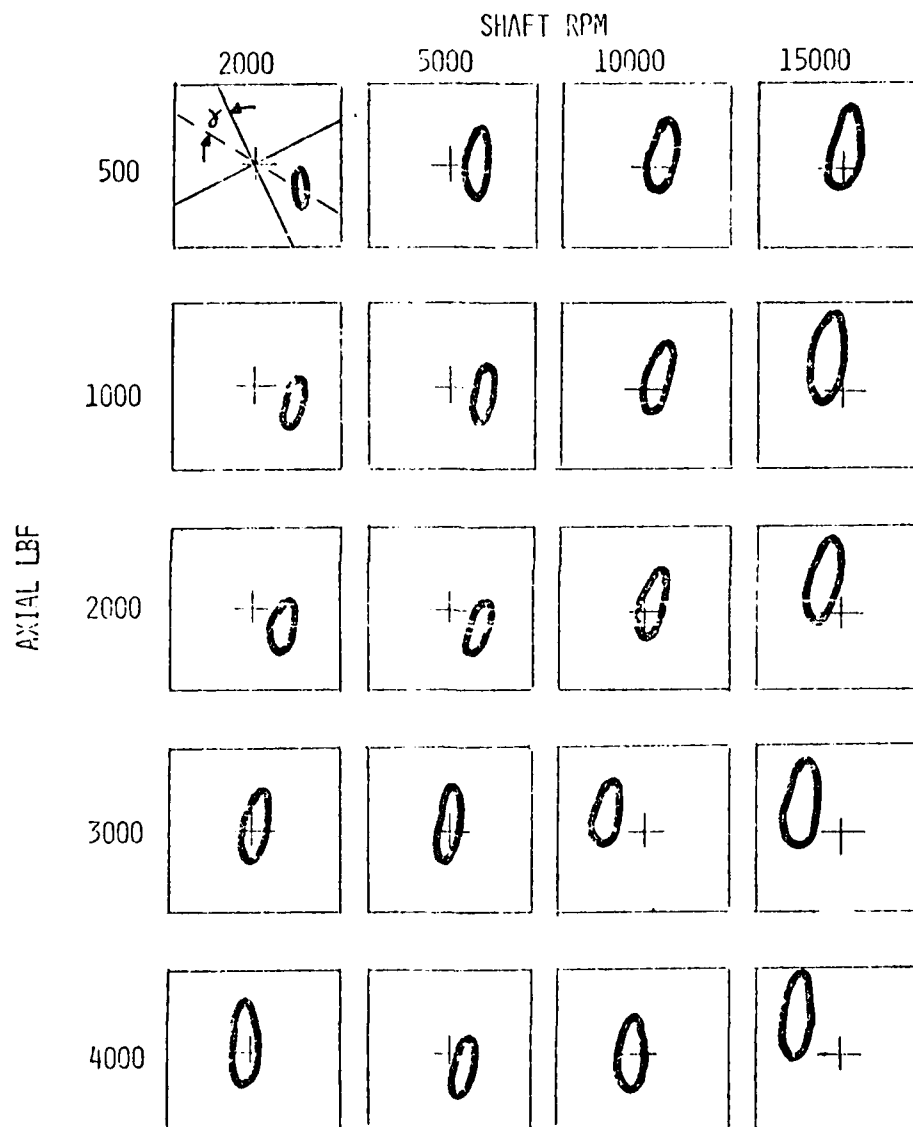


Figure 29. Cage Whirl Images Photographed
on Oscilloscope,
 α = Cage-Inner Ring Contact Angle

The size and location of the Lissajous figures were affected both by an increase in speed and an increase in thrust load. The general elliptical shape and orientation of the major axis was not significantly affected by the increase.

At the smaller loads (2224-8896 N) the size of the Lissajous figures nearly doubled in both axes as the shaft speed was increased from 2,000 to 15,000 rpm. At large loads (13344 and 17292 N) the size of the figures did not grow as substantially with the increased speed. Using the calibration curves for the Bently probes, the actual magnitude of whirl in the major axis ranged from .002 to .006 inches and in the minor axis it ranged from .001 to .003 inches.

The location of the Lissajous figures also was affected by the change of load or speed. Increasing thrust or speed caused the center of the Lissajous figure to traverse about .005 inches in an upward (against gravity) direction, nearly parallel to the z axis. This was expected since the cage started from rest in the lowest position. The rotation of the mass center vector occurred almost as predicted in DREB. The angles in Figure 29 were plotted in Figure 30 to show the relation of inner race/cage angle versus shaft speeds. DREB predicted this angle to increase in the direction of shaft rotation with each increase of shaft speed. Experiment also showed contact angle to move in this direction but the smaller values indicated perhaps that the minimum clearance had started closer to the top of the bearing than predicted by DREB.

Figure 31 shows data (for the 2,000 lbf, 15,000 rpm case) as plotted by DREBP describing the time variation of the cage mass center position in the axial, radial, and orbital directions. The top plot indicates that the cage mass center had whirled about the bearing center almost 3/4 of one revolution during the time interval shown. This interval was about nine milliseconds of real time and represented the last 500 of 990 computer integration steps. During this time interval, the cage had rotated about its own center one full revolution. This means, therefore, that the whirl velocity was slightly less than the orbital velocity.

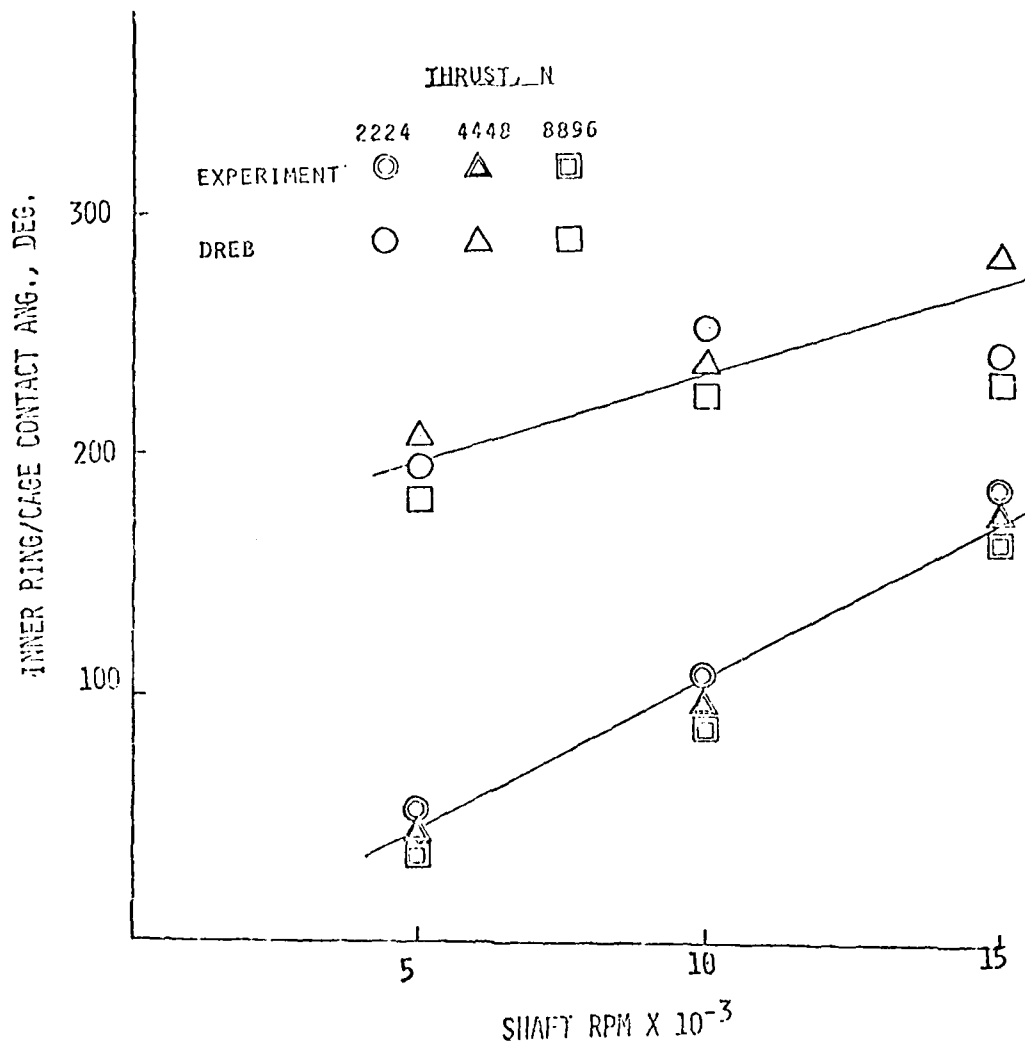


Figure 30. Inner Ring-Cage Contact Angle (α)

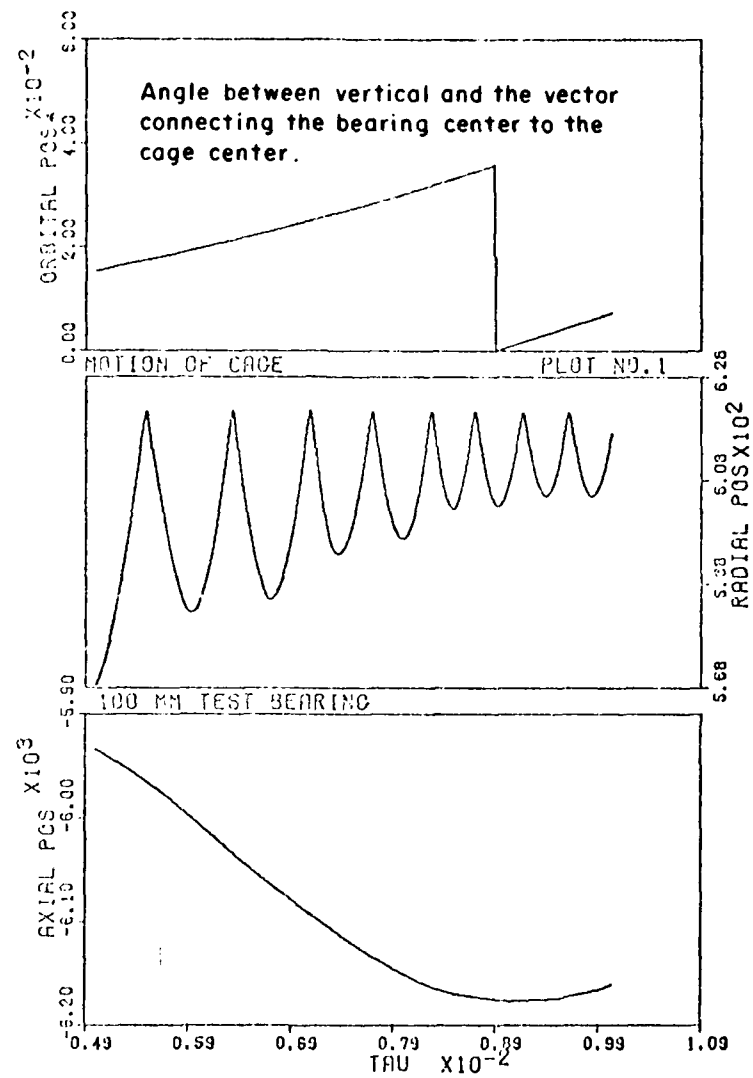


Figure 31. DREBP of Cage Mass Center Position
 Length Scale Factor = 9.52×10^{-3} M
 Time Scale Factor = 1.74×10^{-4} sec.

The middle plot of Figure 31 describes the cage center radial movements. The almost nine peaks represent an oscillation of half the ball-pass frequency, resulting probably from some kind of ball-cage interaction. The peak to peak amplitude of this oscillation was 0.007 inch and apparently was leveling about an average absolute displacement from the bearing center of 0.0229 inch. The cage was rising from its initial eccentric position. The user specified clearance between the cage and the riding surface of the inner ring was 0.0250 inch. Since the ball-cage interaction peaks appear to reach a maximum level of 0.0233 inch it is probable that the cage was bumping the inner ring at half the ball-pass frequency, but that the hydrodynamic film was not penetrated. This sort of cage-ring contact was not observed in the experimental studies.

The bottom plot in Figure 31 shows that the cage mass center moved axially about an average displacement from the bearing center of 0.0023 inch with a periodic displacement of about 0.0001 inch. This periodicity occurred roughly at one-half of the cage orbital frequency. It is possible that the cage center radial motion had this same frequency and that it was 180° out of phase with the axial motion. This can be only determined for certain by running DREB much longer.

Figure 32 shows the cage mass center velocity as calculated by DREB and plotted by DREBP. The top plot shows whirl. This velocity is shown to be somewhat erratic, varying between 4,000 and 6,000 rpm (the shaft speed was 15,000 rpm). The cage orbital speed (again referring to the connotation of orbital speed as used in this study) was shown in Figure 27 to be about 6,800 rpm. Therefore, the top plot of Figure 32 shows the DREB calculated cage whirl velocity to be approaching the DREB calculated orbital velocity. The equivalence of these two velocities is a criterion for bearing stability.

b. Frequency Spectrum Analysis Test Results

The frequency spectra for various load/speed conditions are shown in the Appendix. All of the spectra are characterized with a large peak at or near the cage orbiting frequency. This indicates that

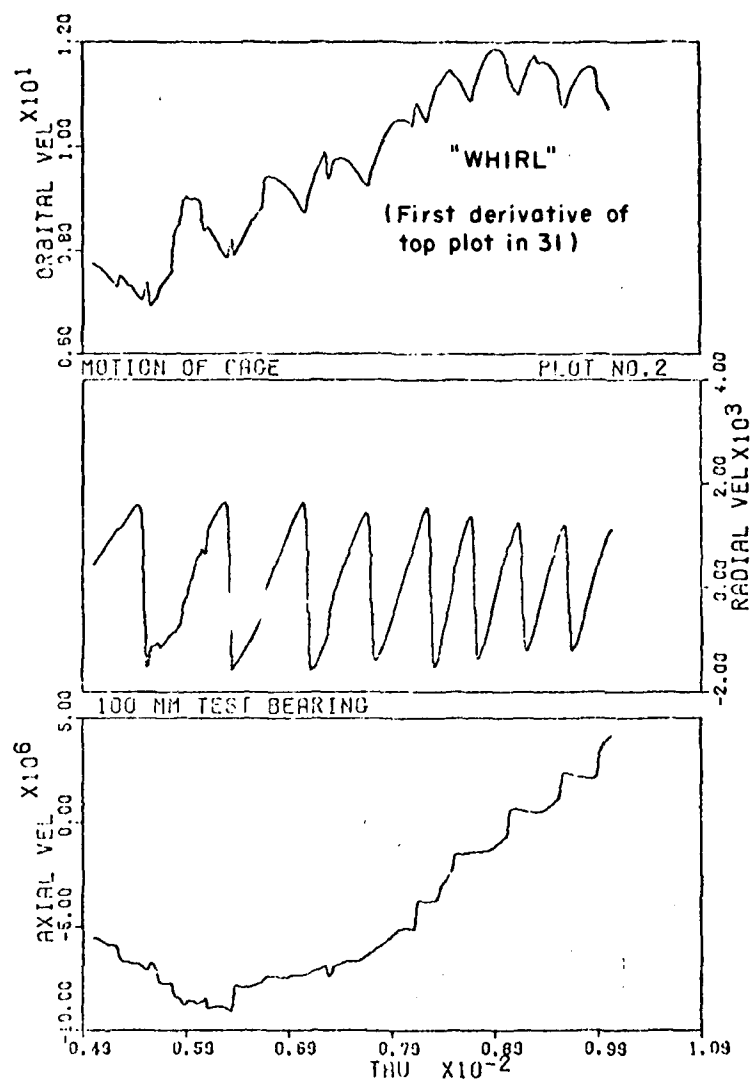


Figure 32. DREBP of Cage Mass Center Velocity
 Vel. Scale Factor = 5.49×10^4 RPM
 Time Scale Factor = 1.74×10^{-4} sec.

the cage mass center was synchronous with the cage rotation. It can be verified that indeed this peak occurred at the cage orbiting frequency by comparison with the ball-pass frequency (18 times the cage frequency) which appeared on the high end of the spectra. This was done but the spectra shown in the Appendix was filtered at a frequency below the ball pass for easier resolution of the lower frequencies.

By plotting the magnitude of the cage whirl vs. the frequency for each probe, a representation of the three-dimensional motions of the cage was obtained. Figures 33 and 34 show the data from both radial probes and two axial probes for five different thrust loads and four different shaft speeds. The actual magnitude of the cage oscillations in inches can be obtained by dividing all radial probe readings by 1.25×10^5 and all axial probe readings by 1.50×10^5 . These sensitivities were derived from the calibration procedure described in Section III.

Figures 33 and 34 show that the amplitude of cage whirl tended to increase in all directions with increasing shaft speed. As was observed in the Lissajous study, this increase was greatest in the radial plane and about twice as great in the vertical axis as in the horizontal axis. The maximum whirl amplitude in the vertical-radial direction was between .004 and .006 inches. The axial probe values (Figure 10) were generally more erratic and smaller in magnitude than the radial displacements. Both Figures 33 and 34 show a convergence of data at 80 hz., the frequency corresponding to a cage speed of 4,800 rpm and a shaft speed of about 9,000 rpm. As already noted, it is possible that this frequency region identifies the beginning of full-film lubrication in the ball-race contacts and/or between the cage and inner ring. It should be noted that the noise level on each spectrum was less than 10% of the cage frequency amplitudes. Also, the amplitudes of the shaft rotational frequencies were generally lower than the 100 mV level.

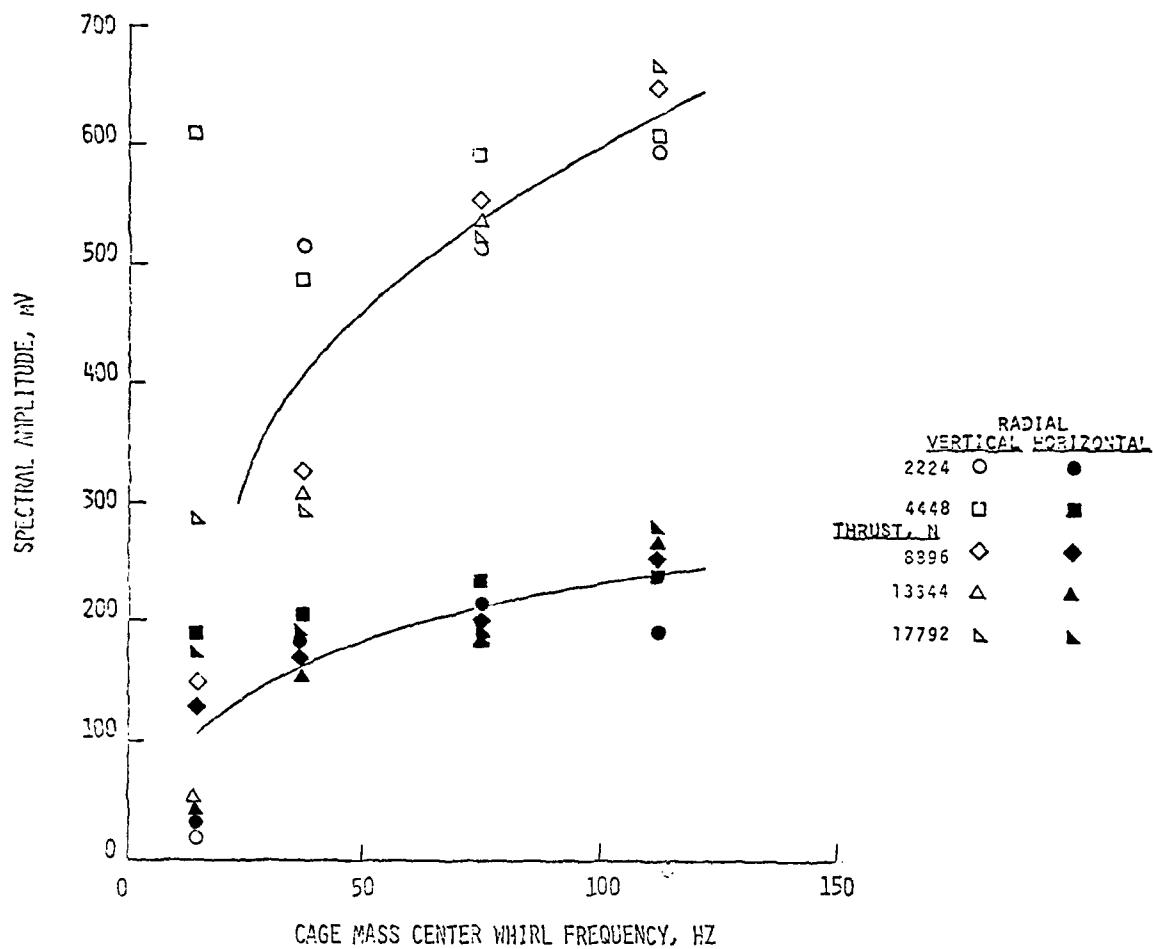


Figure 33. Cage Radial Motion in Vertical and Horizontal Directions

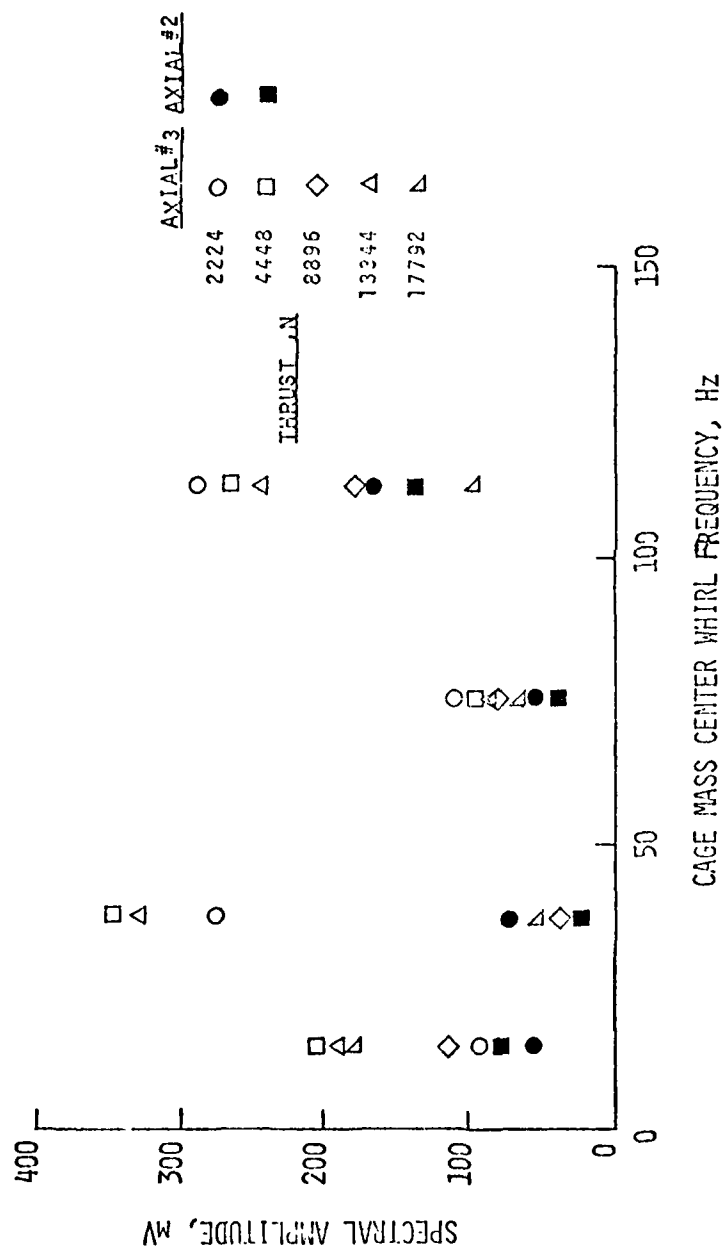


Figure 34. Cage Axial Motion

SECTION V

CONCLUSIONS AND RECOMMENDATIONS

The conclusion reached by this study was that SHABERTH was more practical than DREB as a preliminary bearing design tool. This was based on the ability of SHABERTH to calculate reasonable fatigue life, torsion, and heat generation values and to do so with much less computer and programmer's time than DREB.

Despite the inherent slowness of DREB, however, its dynamic analysis demonstrated potentially great value as a diagnostic tool. Disappointingly incomplete information about the bearing kinematics was obtained from DREB because of the prohibitively large amounts of computer time it consumed. Nevertheless, some of the experimental trends describing cage motion were upheld by the DREB analysis.

The test bearing used in this study was observed to perform very well for the range of speeds and loads tested. No excessive levels of vibration, heat generation or torque were measured for this bearing as compared to typical behavior of turbine engine, main shaft thrust bearings. The design limits of this bearing, however, were never really tested. Future studies should include tests to at least 2.5 million DN with loads over 4,000 lbf.

DREB produced perhaps some unnecessary output. Methods for decreasing the number of computations but retaining most of the accuracy probably must be found before the program can be more widely used by bearing designers. Perhaps the program should only print the most important results, especially the overall parameters describing performance. It should not print output which is so time-dependent that the instantaneous values are misleading (cage whirl velocity for example). The plotting routine, DREBP, is wholly sufficient for this purpose.

Although the addition of a thermal routine in DREB would provide more information in the output, the increased length of the program probably would not warrant such an addition. If thermal data is

desired, then one should use SHABERTH. Likewise, the inclusion into SHABERTH of a dynamic analysis of the cage balls probably should not be done since its economical advantage would have to be sacrificed. If one is studying the dynamics of the balls and/or cage, then one should use DREB.

In future studies it is recommended that enough computer time be allotted to DREB to run a more complete dynamic analysis. It would be interesting to model a bearing with an unbalanced cage and then to compare the results to experimentation of a test bearing with the same cage unbalance. Preliminary tests have been conducted with the system described in this report using a cage with a flange on both sides of the outer diameter perimeter, to provide the radial Bently probes with a wider target in order to increase the sensitivity. This and other improvements for measuring cage motion are being developed at WPAFB in an effort to understand the complex phenomena occurring inside the bearing during operation.

AFWAL-TR-80-2007

APPENDIX

FREQUENCY SPECTRA FOR MOTION OF
THE CAGE IN THE 100 mm TEST BEARING

PRECEDING PAGE BLANK-NOT FILMED

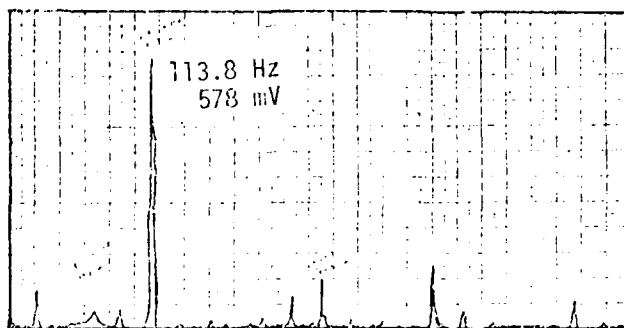
RADIAL PROBE #5
2224 N (500 Lbf) Thrust

Frequency
Range

Shaft
Speed

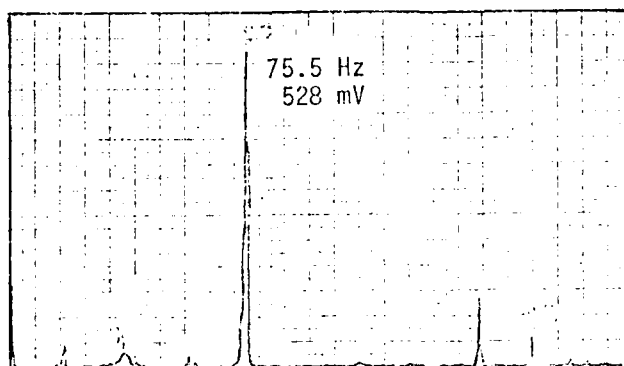
0-500 Hz

250 Hz



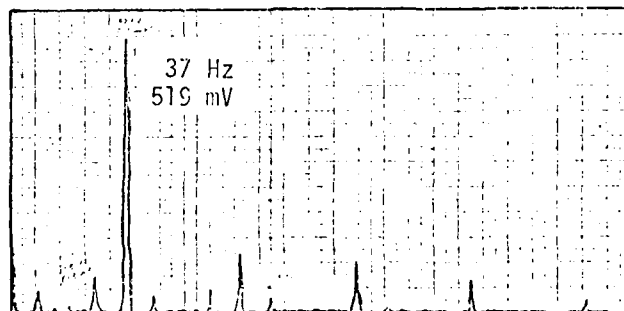
0-200 Hz

167 Hz



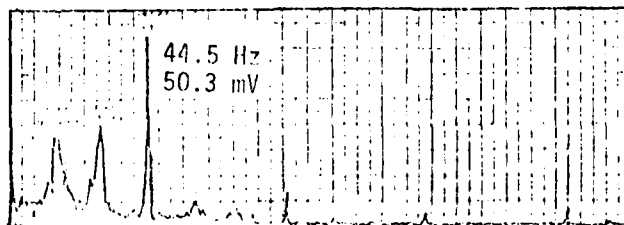
0-200 Hz

84 Hz



0-200 Hz

33 Hz



AFWAL-TR-80-2007

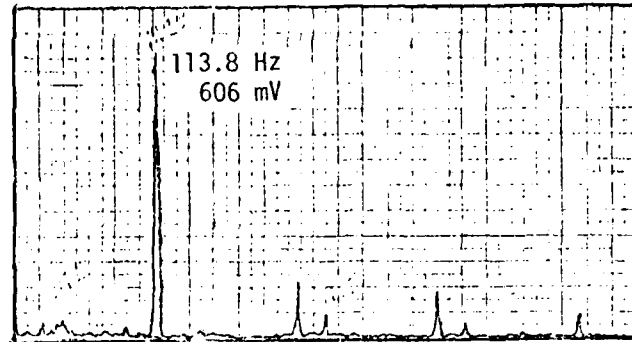
RADIAL PROBE #5, 4448 N (1000 Lbf) Thrust

Frequency
Range

Shaft
Speed

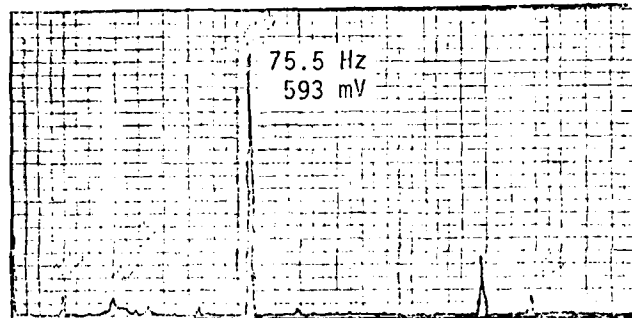
0-500 Hz

254 Hz



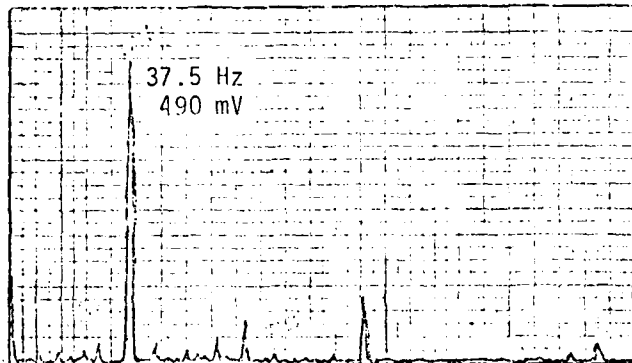
0-200 Hz

167 Hz



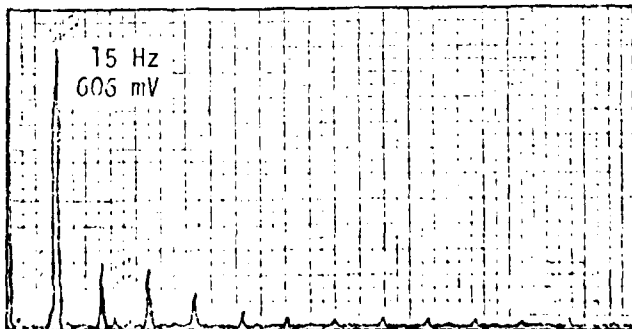
0-200 Hz

84 Hz



0-200 Hz

33 Hz



AFWAL-TR-80-2007

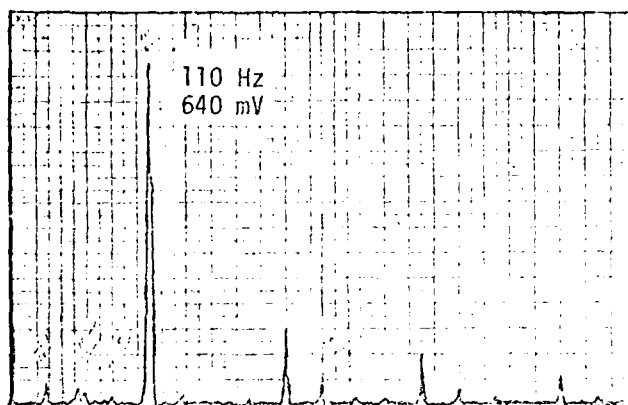
RADIAL PROBE #5
8896 N (2000 Lbf) Thrust

Frequency
Range

Shaft
Speed

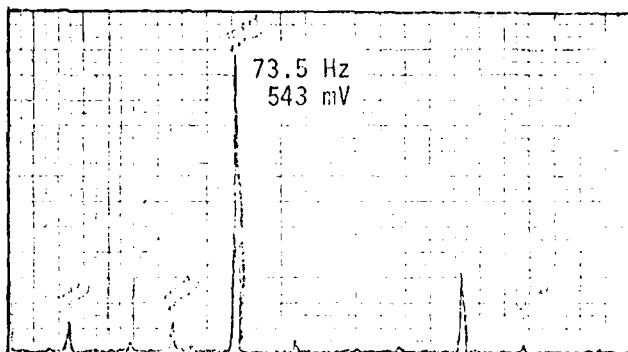
0-500 Hz

250 Hz



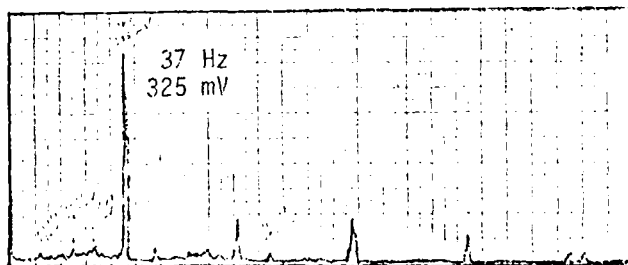
0-200 Hz

167 Hz



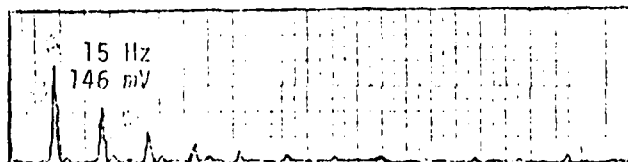
0-200 Hz

84 Hz



0-200 Hz

33 Hz



AFWAL-TR-80-2007

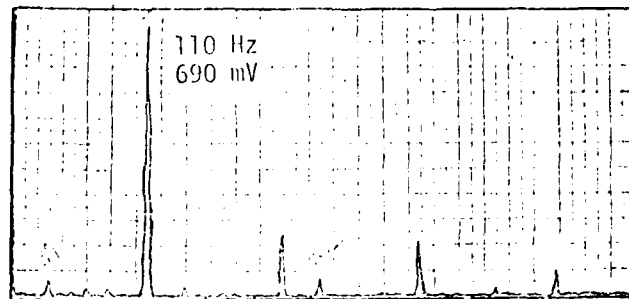
RADIAL PROBE #5
13,344 N (3000 Lbf) Thrust

Frequency
Range

Shaft
Speed

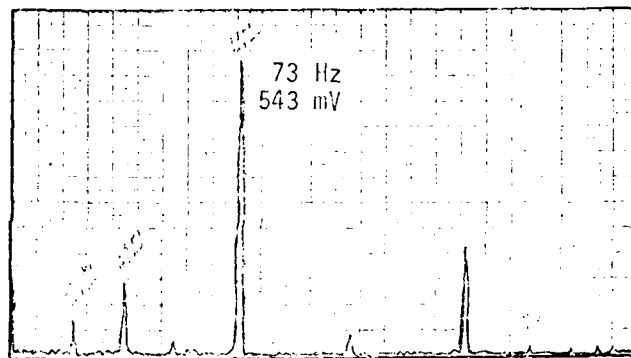
0-500 Hz

250 Hz



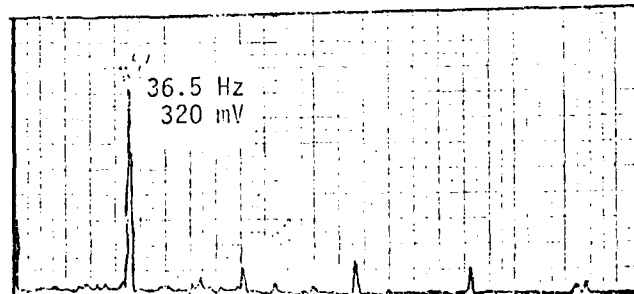
0-200 Hz

167 Hz



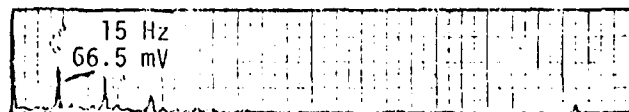
0-200 Hz

84 Hz



0-200 Hz

33 Hz



AFWAL-TR-80-2007

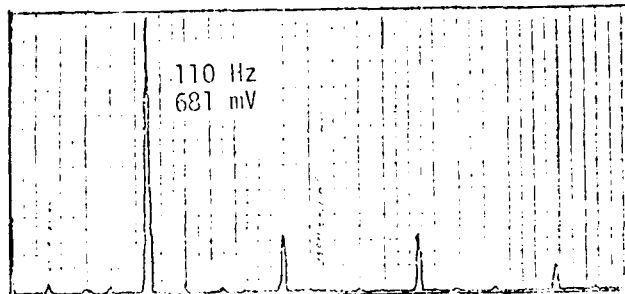
RADIAL PROBE #5
17,792 N (4000 Lbf) Thrust

Frequency
Range

Shaft
Speed

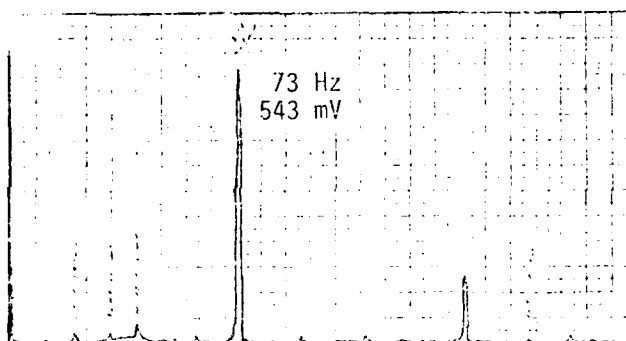
0-500 Hz

250 Hz



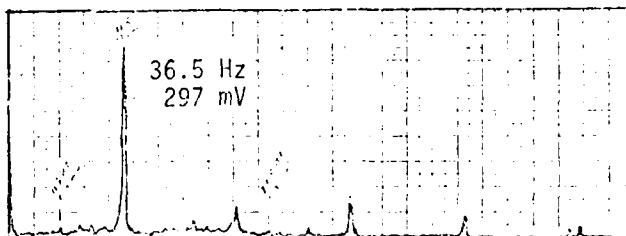
0-200 Hz

167 Hz

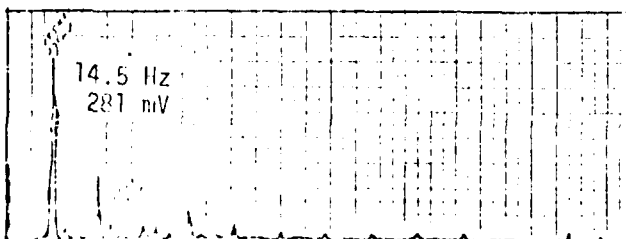


0-200 Hz

84 Hz



53 Hz



AFWAL-TR-80-2007

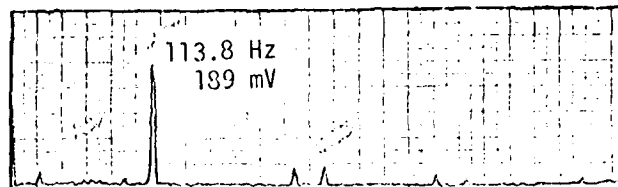
RADIAL PROBE #4
2224 N (500 Lbf) Thrust

Frequency
Range

Shaft
Speed

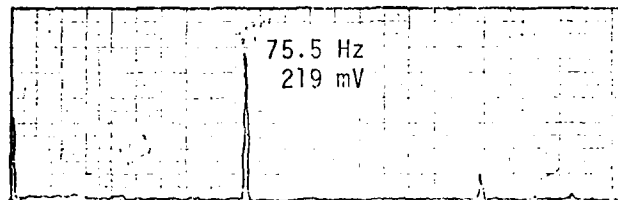
0-500 Hz

750 Hz



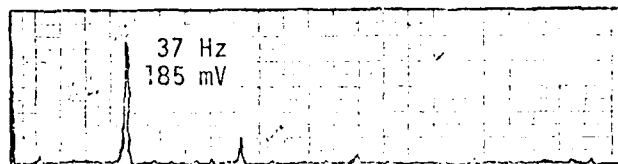
0-200 Hz

167 Hz



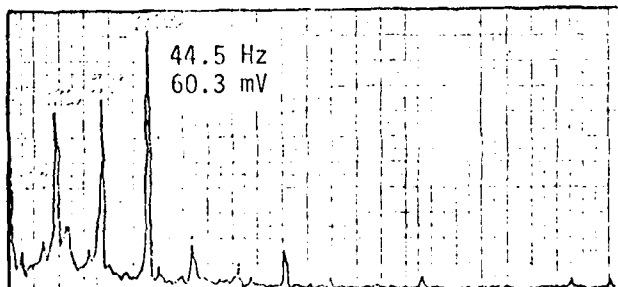
0-200 Hz

84 Hz



0-200 Hz

33 Hz



AFWAL-TR-80-2007

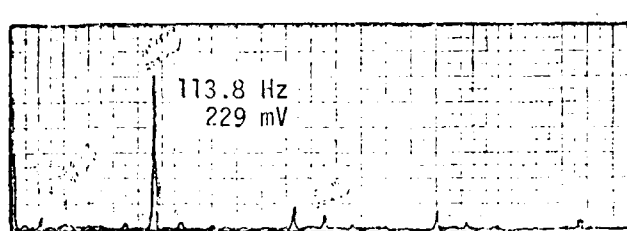
RADIAL PROBE #4
4448 N (1000 Lbf) Thrust

Frequency
Range

Shaft
Speed

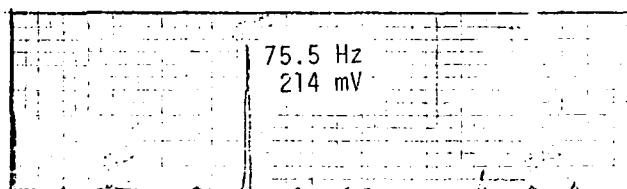
0-500 Hz

250 Hz



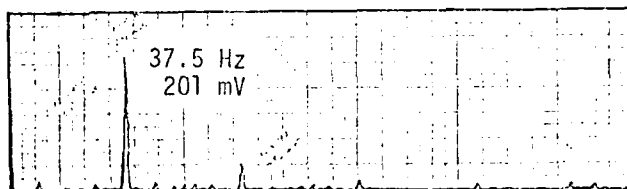
0-200 Hz

167 Hz



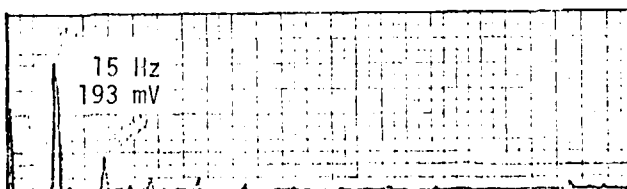
0-200 Hz

84 Hz



0-200 Hz

33 Hz

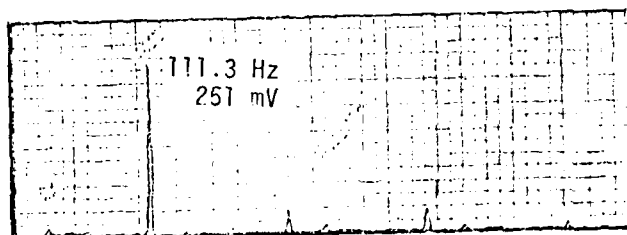


AFWAL-TR-80-2007

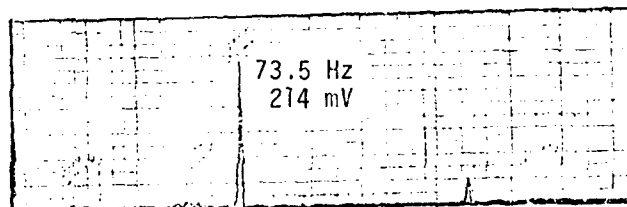
RADIAL PROBE #4
8896 N (2000 Lbf) Thrust

<u>Frequency Range</u>	<u>Shaft Speed</u>
----------------------------	------------------------

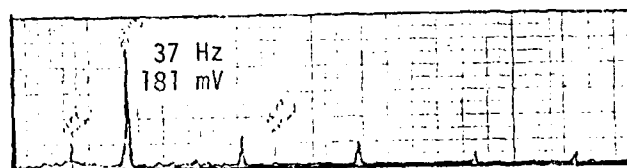
0-500 Hz	250 Hz
----------	--------



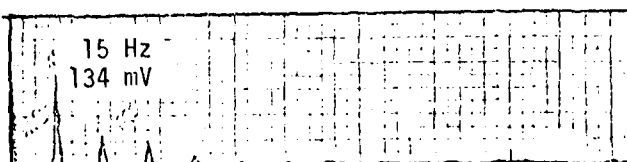
0-200 Hz	167 Hz
----------	--------



0-200 Hz	84 Hz
----------	-------



0-200 Hz	33 Hz
----------	-------



AFWAL-TR-80-2007

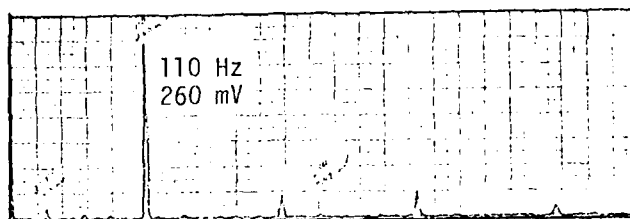
RADIAL PROBE #4
13,344 N (3000 Lbf) Thrust

Frequency
Range

Shaft
Speed

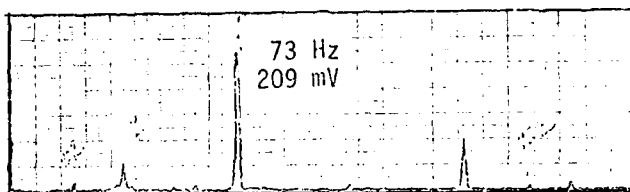
0-500 Hz

250 Hz



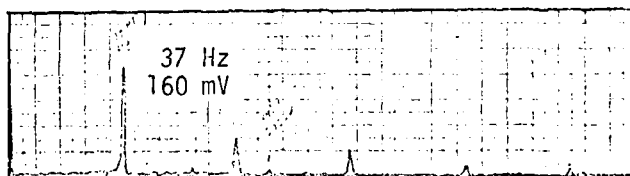
0-200 Hz

167 Hz



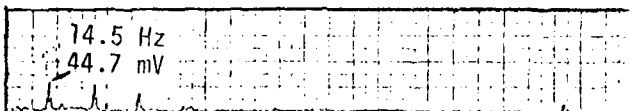
0-200 Hz

84 Hz



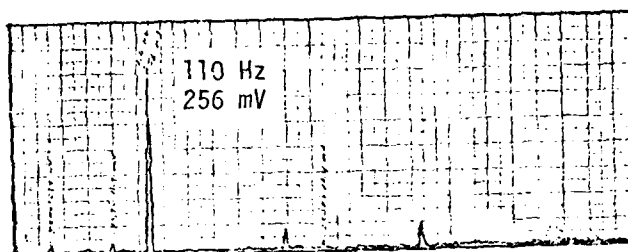
0-200 Hz

33 Hz

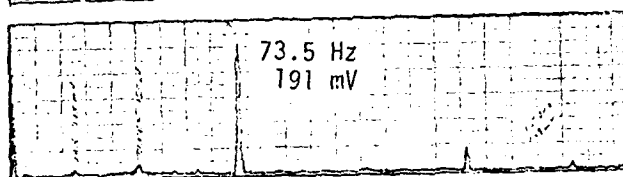


RADIAL PROBE #4
17,792 N (4000 Lbf) Thrust

Frequency Range	Shaft Speed
0-500 Hz	250 Hz



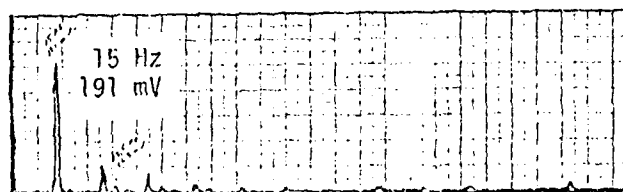
0-200 Hz	167 Hz
----------	--------



0-200 Hz	84 Hz
----------	-------



0-200 Hz	33 Hz
----------	-------



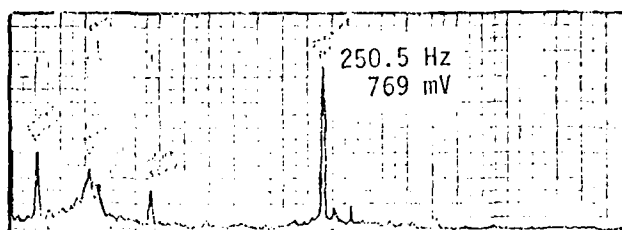
AXIAL PROBE #3
2224 N (500 Lbf) Thrust

Frequency
Range

Shaft
Speed

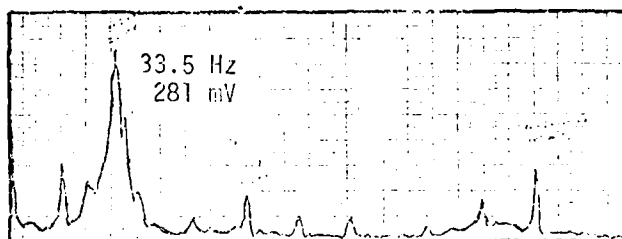
0-500 Hz

250 Hz



0-200 Hz

167 Hz



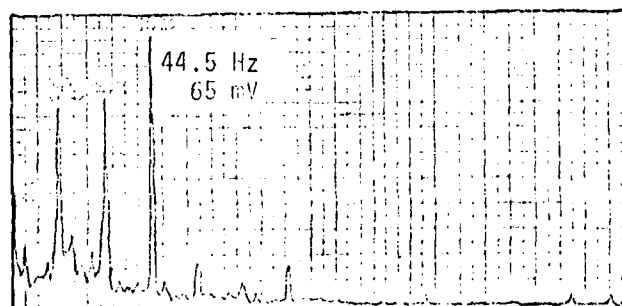
0-200 Hz

84 Hz



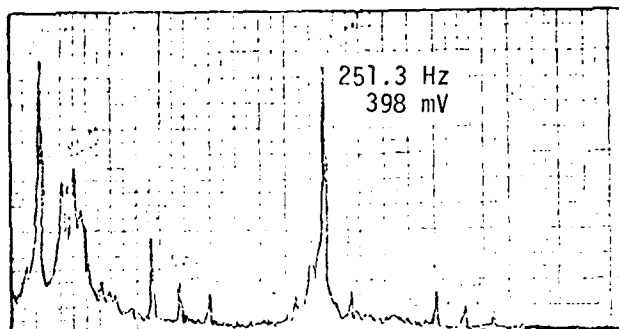
0-200 Hz

33 Hz

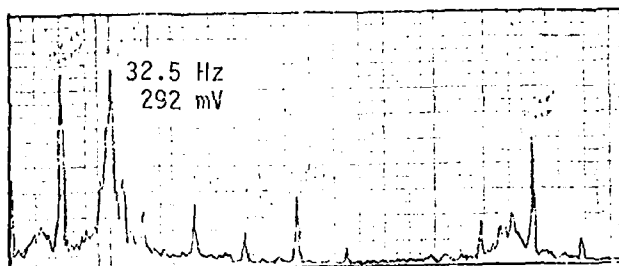


AXIAL PROBE #3
4448 N (1000 Lbf) Thrust

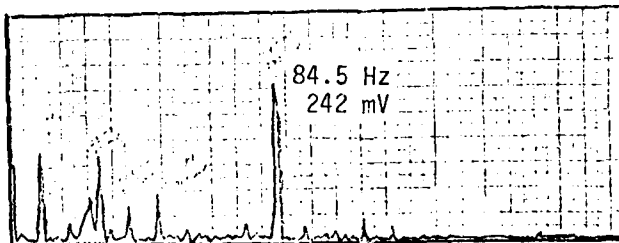
Frequency Range	Shaft Speed
0-500 Hz	250 Hz



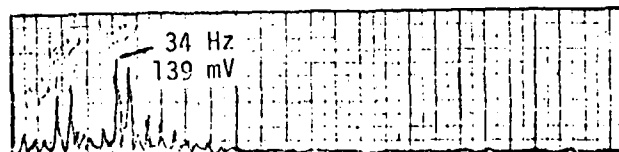
0-200 Hz	167 Hz
----------	--------



0-200 Hz	84 Hz
----------	-------



0-200 Hz	33 Hz
----------	-------



AFWAL-TR-80-2007

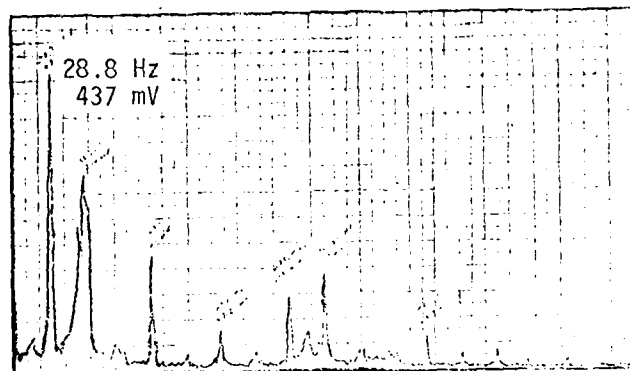
AXIAL PROBE #2
8896 N (2000 Lbf) Thrust

Frequency
Range

Shaft
Speed

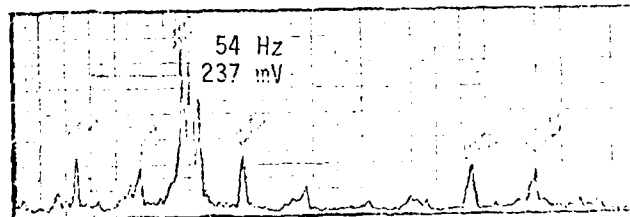
0-500 Hz

250 Hz



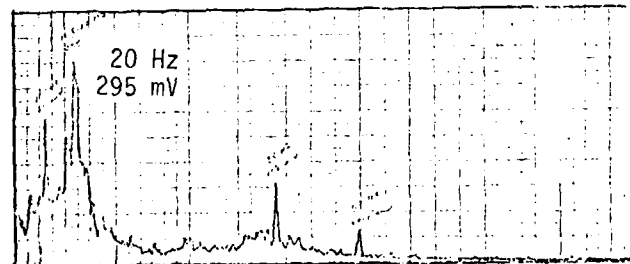
0-200 Hz

167 Hz



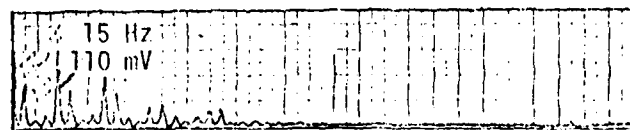
0-200 Hz

84 Hz



0-200 Hz

33 Hz



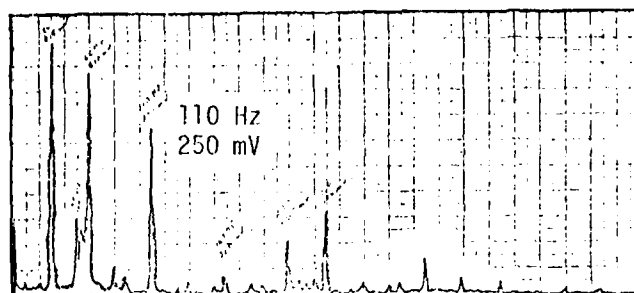
AXIAL PROBE #2
13,344 N (3000 Lbf) Thrust

Frequency
Range

Shaft
Speed

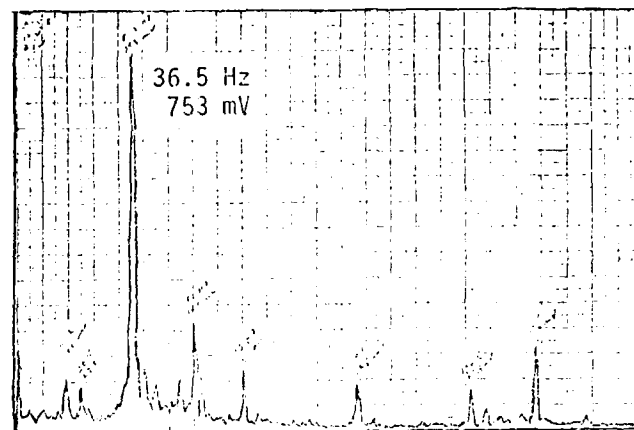
0-500 Hz

250 Hz



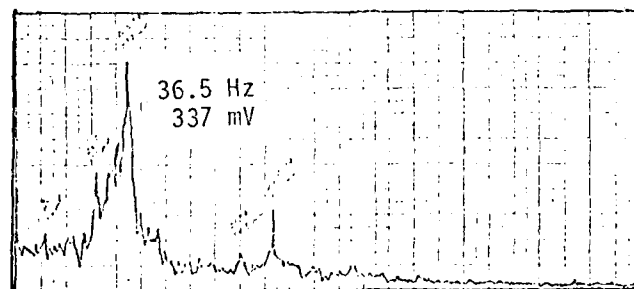
0-200 Hz

167 Hz



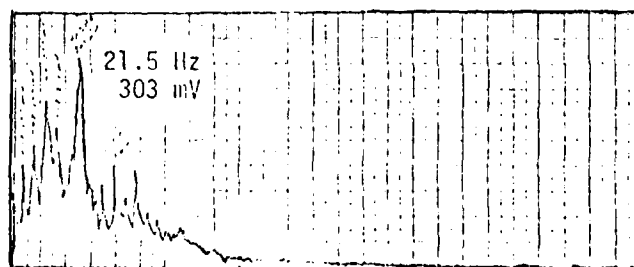
0-200 Hz

84 Hz



0-200 Hz

33 Hz



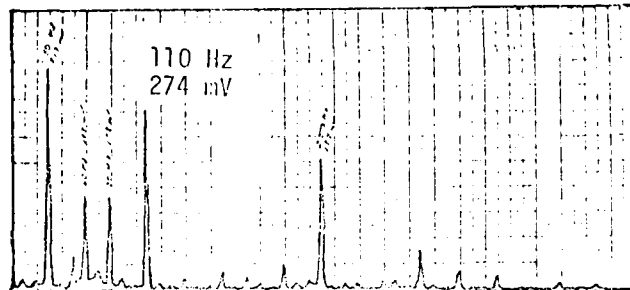
AXIAL PROBE #2
17,792 N (4000 Lbf) Thrust

Frequency
Range

Shaft
Speed

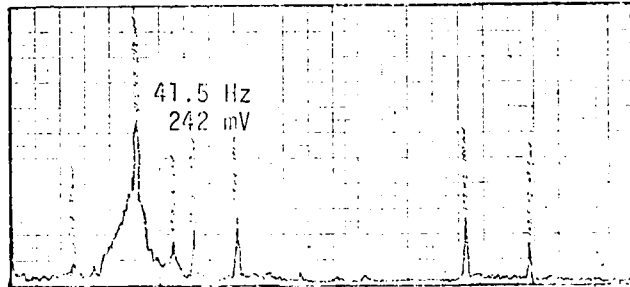
0-500 Hz

250 Hz



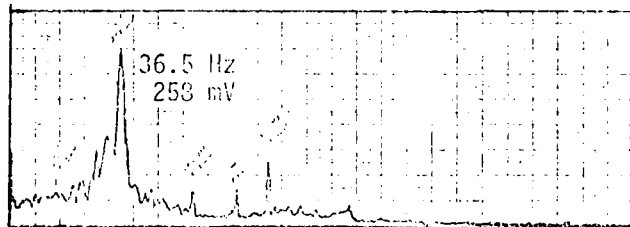
0-200 Hz

167 Hz



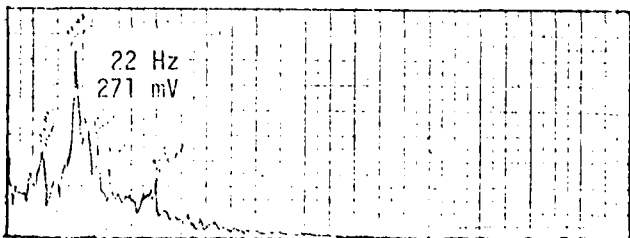
0-200 Hz

84 Hz



0-200 Hz

33 Hz



REFERENCES

1. Kannel, J. W., Snediker, D. K., "The Hidden Cause of Bearing Failures," Machine Design, Vol. 49, No. 8, April 1977
2. Kannel, J. W., Dechow, J. P., Walters, C. T., "Analysis of Separator Dynamics in Low Speed Despun Antenna Bearings," Proc. Intern Ball Bearing Symposium, C. S. Draper Lab., June 1973
3. Coe, H. C., Zaretsky, E. V., Predicted and Experimental Performance of Jet-Lubricated 120 mm Ball Bearings, Operating to 2.5 million DN, NASA Tech. Paper 1196, April 1978
4. Walters, C. T., "The Dynamics of Ball Bearings," Journ. of Lub. Tech., ASME Trans., Jan. 1971
5. Gupta, P., "Vibrational Characteristics of Ball Bearings," Journ. Lub. Tech., April 1977
6. SKF Industries, Inc., Computer Program Operation Manual on 'SHABERTH' --A Computer Program for the Analysis of the Steady State and Transient Thermal Performance of Shaft/Bearing Systems, USAF Tech. Report AFAPL-TR-76-90
7. Crecelius, W. J., Heller, S., Chiu, Y. P., Improved Flexible Shaft-Bearing Thermal Analysis with NASA Friction Models and Cage Effects, SKF Report No. AL76P003, Feb. 1976
8. Gupta, P. K., Dynamics of Rolling Element Bearings - Part I: Analysis of Cage Motion, MTI TECH REPORT, MTI 76 TR 42, June 1976
9. Gupta, P. K., Dynamics of Rolling Element Bearings, Part II: Analysis of Ball Motion, MTI TECH REPORT, MTI 76 TR 44, June 1976
10. Gupta, P. K., Dynamics of Rolling Element Bearings, Part IV: EHD Traction and Other Factors, TECH REPORT, MTI 77 TR 51, June 1977
11. Gupta, P. K., Dynamics of Rolling Element Bearings, Part VI: Computer Program Manual, MTI TECH REPORT, MTI 77 TR 55, June 1977

BIBLIOGRAPHY

Allen, C. W., Townsend, D. P., Zaretsky, E. V., "EHD Lubrication of a Spinning Ball in a Nonconforming Groove," Journ. Lubrication Tech., ASME Trans., Jan. 1970

Archard, J., Cowking, E., "EHD Lubrication at Point Contacts," Proc. Inst. Mech. Eng., 1965-66

Bamberger, E. N., Harris, T. A., Kacmarsky, W. M., Moyer, C. A., Parker, R., Sherlock, J. T., Zaretsky, E. V., Life Adjustment Factors for Ball and Roller Bearings, ASME Publication, 1971

Boness, "The Effect of Oil Supply on Cage and Roller Motion in a Lubricated Roller Bearing," Journ. Lub. Tech. ASME Trans., Jan. 1970

Chiu, U. P., "An Analysis and Prediction of Lubricant Film Starvation in Rolling Contact Systems," ASME Trans. 1971

Dowson, D., Higgison, G. R., Elastohydrodynamic Lubrication, Pergamon Press, 1966

Dowson, D., Higgison, G. R., "Theory of Roller Bearing Lubrication and Deformation," Proc. Inst. Mech. Eng., London, 1963

Floberg, L., Lubrication of Two Cylindrical Surfaces Considering Cavitation, Report No. 14, Chalmers Univ. of Tech., Gothenburg, 1966

Ford, "The Effects of EHD Traction Behavior on Cage Slip in Roller Bearings," Journ. Lub. Tech., Trans. ASME, July 1974

Hamrock, B. J., Dowson, D., "Isothermal EHD Lubrication of Point Contacts, Part III - Fully Flooded Results," Journ. Lub. Tech., ASME Trans, April 1977

Harris, T. A., "An Analytical Method to Predict Skidding in Thrust Loaded Angular Contact Ball Bearings," Journ. Lub. Tech., ASME Trans., 1971

Harris, T. A., Rolling Bearing Analysis, John Wiley and Sons, 1966

Johnson, K. L., Cameron, R., "Shear Behavior of EHD Oil Film at High Rolling Contact Pressures," Proc. Inst. Mech. Eng., London, 1967-68

Kannel, J. W., Bupara, S. S., "A Simplified Model of Cage Motion in Angular Contact Bearings Operating in the EHD Lubrication Regime," Journ. Lub. Tech., ASME Trans, July 1978

Kingsbury, E. P., Torque Variations in Instrument Ball Bearings, Tech. Report No. E-1675, C. S. Draper Lab., June 1964

BIBLIOGRAPHY (Cont'd)

Knudsen, J. G., Katz, D. L., Fluid Dynamics and Heat Transfer, McGraw-Hill Book Co., New York

Lin, J. Y., Tallian, T. E., McCool, J. I., Dependence of Bearing Fatigue Life on Film Thickness to Surface Roughness Ratio, ASLE Preprint 74AM-7B-1, 1974

Loewenthal, S. H., Parker, R. J., Zaretsky, E. V., Correlation of EHD Film Thickness Measurements for Fluoro-carbon Type II Ester and Polyphenyl Ether Lubricants, NASA Tech. Note D-7825, 1974

Lundberg, G., Palmgren, A., "Dynamic Capacity of Roller Bearings," Proc. Royal Swedish Acad. Eng., Vol. 2, No. 4, 1952

Lundberg, G., Palmgren, A., "Dynamic Capacity of Rolling Bearings," Acta Polytechnica, Mech. Eng. Series 1, Proceedings Royal Swedish Acad. Eng., Vol. 7, No. 3, 1947

McCool, J. I., Influence of EHD Lubrication on the Life and Operation of Turbine Engine Ball Bearings - Bearing Design Manual, Wright-Patterson AFB, OH, Tech. Report AFAPL-TR-75-25, May 1975

McGrew, J. M., Gu, A., Ching, H. S., Murray, S. F., EHD Lubrication - Preliminary Design Manual, Wright-Patterson AFB, OH, Tech. Report AFAPL-TR-70-27, Nov. 1970

Nypan, L. J., Study of Rolling Element Dynamic Interactions with Separators and Raceway Paths, Ball to Separator Contact Forces in Angular Contact Ball Bearings under Thrust and Radial Loads, Cal. State Univ., Status Report NSG 3065, NASA, July 1977

Pentlicki, C. J., Investigation of the INTELSAT IV Bearing and Power Transfer Assembly, COMSAT Tech. Rev., Vol. 3, No. 1, 1973

Pinkus, O., Sternlicht, B., Theory of Hydrodynamic Lubrication, McGraw-Hill, 1961

Rumbarger, J. H., Dunfee, J. D., Survey of the State-of-the-Art for the Design of High Speed Rolling Element Bearings Used in Gas Turbine Engines, Tech. Report F-C2138-1, Vol II, Nav. Air Propulsion Test Center, Feb 1969

Signer, H., Bamberger, E. N., Zaretsky, E. V., "Parametric Study of the Lubrication of Thrust Loaded 120-mm Bore Ball Bearings to 3 Million DN," Journ. Lub. Tech. Trans. ASME, July 1974

Smith, R. L., Walowit, J. A., Gupta, P. K., McGrew, J. N., Research on EHD Lubrication of High Speed Rolling-Sliding Contacts, Wright-Patterson AFB, OH, Tech. Report AFAPL-TR-72-56, July 1972

AD-A089 161

AIR FORCE WRIGHT AERONAUTICAL LABS WRIGHT-PATTERSON AFB OH F/G 21/5
AN EVALUATION OF THE USEFULNESS OF TWO MATH MODELS FOR PREDICTI--ETC(U)
APR 80 D R SCHULZE
AFWAL-TR-80-2007

UNCLASSIFIED

NL

2 of 2
40-1001



END
DATE
FILMED
40-80
DTIC

BIBLIOGRAPHY (Concluded)

Smith, R. L. Walowit, J. A., McGrew, J. M., "EHD Traction Characteristics of 5P4E Polyphenyl Ether," Journ. Lub. Tech., ASME Trans., July 1973

Townsend, "Study of Ball Bearing Torque under EHD Lubrication," Journ. Lub. Tech., Trans. ASME, Oct. 1974

Walowit, J. A., Smith, R. L., "Traction Characteristics of MIL-L-7808 Oil," Journ. Lub. Tech., ASME Trans., Oct. 1976

Wolveridge, P. E., Baglin, K. P., Archard, J. F., "The Starved Lubrication of Cylinders in Line Contact," Proc. Inst. Mech. Eng., Vol. 185, London, 1970-71